TiS Trends in Sciences
TRENDS IN SCIENCES 2027; 24(1): 14202
SPRINT Scholarly Publishing and Repository Integration Center
https://doi.org/10.48048/tis.2027.14202
RESEARCH ARTICLE

Novel Insights into Anti-proliferative Activity of *Nepenthes mirabilis* and Its Constituents on HeLa Cervical Cancer Cells

Thanh Quoc Chau Nguyen[1,2], Tue Minh Duong[3], Nguyen Trong Tuan[4], Duy Binh Tran[5], Tuan Le Anh Pham[6], Tomonori Waku[3], Kenji Kanaori[3] and Kaeko Kamei[3,*]

[1]*Faculty of Chemistry, College of Natural Sciences, Can Tho University, Can Tho, Vietnam*
[2]*Bioassay Laboratory, CTU Hi-tech Building, Can Tho University, Can Tho, Vietnam*
[3]*Department of Functional Chemistry, Kyoto Institute of Technology, Kyoto, Japan*
[4]*Faculty of Health Sciences, College of Natural Sciences, Can Tho University, Can Tho, Vietnam*
[5]*Division of Surgical Oncology, University of Illinois College of Medicine, Chicago, Illinois, USA*
[6]*Department of Molecular Pathology, Ha Noi Medical University, Ha Noi, Vietnam*

([*]Corresponding author's e-mail: kaeko.kamei313@gmail.com)

Received: 27 April 2026, Revised: 12 June 2026, Accepted: 22 June 2026, Published: 30 August 2026

Abstract

Nepenthes mirabilis, a carnivorous plant species predominantly distributed across tropical regions, has long been utilized in ethnomedicine to treat various ailments. However, mechanistic evidence regarding its anticancer activity, particularly against cervical cancer cells, remains limited. This study sought to evaluate the anti-proliferative effects of *N. mirabilis* methanol extract and its isolated constituent against HeLa cervical cancer cells. The methanol extract showed cytotoxicity against HeLa cells (IC_{50}, 59.33 µg/mL) and a lesser effect on HEK293 cells, resulting in a selectivity index of 3.82. Additionally, the extract impaired clonogenic survival and cell migration, correlating with intracellular ROS accumulation and decreased mRNA expression of Akt and Bcl-2. Bioactivity-guided isolation identified 4 constituents, namely nepenthone C, gallic acid, quercetin, and daucosterol, whereas gallic acid and daucosterol were first reported in this species. Among them, nepenthone C showed the greatest selectivity toward HeLa cells compared with HEK293 cells (IC_{50}, 43.54 µM; SI, 6.44). Mechanistically, nepenthone C induced apoptosis, as evidenced by increased Annexin V-positive apoptotic cell populations, enhanced cleaved caspase-3 activation, reduced Bcl-2 expression, and an elevated Bax/Bcl-2 ratio. The partial rescue effect observed with N-acetyl-L-cysteine (NAC) further suggests that ROS accumulation contributes to nepenthone C-mediated apoptosis, at least partially upstream. Taken together, these findings identify nepenthone C as the major bioactive ingredient responsible for the anti-proliferative activity of *N. mirabilis* and provide initial mechanistic evidence that this natural napthoquinone scaffold promotes ROS-associated mitochondrial apoptosis. This study illustrates that nepenthone C should be considered as a promising candidate for further research into its potential as an anti-cervical cancer agent.

Keywords: Anticancer, Carnivorous plants, Cervical cancer cell, *Nepenthes mirabilis*, Nepenthone

Introduction

Nepenthes mirabilis, commonly known as a carnivorous species belonging to the Nepenthaceae family, absorbs nutrients due to its specific ability through trapping and digesting insects [1]. Indeed, pitcher plants emit a mixture of various volatile secondary metabolites from their flowers and trap scents to attract prey insects [2]. This behavior also enables them to adapt well to diverse habitats, especially nutrient-poor environments. Their geographical distribution is primarily limited to tropical regions of Southeast Asia, with significant populations in Vietnam, Indonesia, and Thailand. Another point is that,

botanically and ecologically, they offer considerable value as potential sources for both chemical and medical research. *Nepenthes mirabilis*'s unique growth process and nutritional characteristics lead to the biosynthesis of diverse secondary metabolites with pharmacological potential [3,4]. It should be noted that seasonal changes and the biodiversity of insect populations are the primary factors driving variations in and distributions of chemical components [5,6]. Hence, a wide range of secondary metabolites from *Nepenthes* species, including flavonoids, naphthoquinones, triterpenoids, steroids, and aliphatic compounds, has been reported [7,8]. These metabolites have been associated with anti-inflammatory, antioxidant, antibacterial, antidiabetic, anti-aging, and cytotoxic effects against several cancer cell lines [3,7-11]. Nevertheless, the anticancer mechanism of *Nepenthes mirabilis* and its constituents remains insufficiently explored, particularly in cervical cancer models.

On the other hand, cervical cancer treatment, depending on the stage and progression of disease, may involve surgery, radiation, and/or the combination of immunotherapy and chemotherapy. This could lead to resistance, severe side effects, and high treatment costs [12]. As a result, extensive research on alternative treatments is needed, and natural products could be a promising complementary source for anticancer drug discovery. Natural products, with diverse structures and that impact multiple cellular pathways, have historically served as scaffolds for anticancer drugs. Most evidence suggests that up to 60% of anticancer drugs in clinical trials are derived from plants [13]. Therefore, bioactivity-guided investigation of medicinal and underexplored plants remains a valuable strategy for identifying potential anticancer molecules. Based on our previous screening, *Nepenthes mirabilis* extract exhibited selectivity toward HeLa cervical cancer cells compared with non-cancerous and other cancer cell lines [11]. However, the active constituents responsible for this effect and their underlying mechanisms have not been fully characterized. In this study, we aimed to address the lack of scientific data regarding the anti-proliferative activity of *N. mirabilis* and its constituents against HeLa cervical cancer cells. Moreover, this study is the first to identify nepenthone C as one of the primary active compounds responsible for *N. mirabilis*'s anti-proliferative effects on HeLa cervical cancer cells, achieved through bioactivity-guided isolation and mechanistic validation. Unlike previous research that broadly focused on the phytochemical profiles or general biological activities of Nepenthes species, our work specifically connects a naphthoquinone constituent to ROS-associated mitochondrial apoptosis in a cervical cancer cell model. Taken together, these findings and hypothesis-generating results provide mechanistic insight into a promising natural naphthoquinone scaffold from N. mirabilis for further investigation into anti-cervical cancer activity.

Materials and methods

Plant material

Fresh samples of *Nepenthes mirabilis* (NM) were collected from Phu Quoc National Park, Phu Quoc Island, Vietnam (coordinates: Latitude, 10°19′30″N and Longitude, 103°57′0″E) during January 2023. The taxonomic identification of the specimens was carried out by Assoc. Prof. Dang Minh Quan (School of Education, Can Tho University, Vietnam). The specimen with herbarium barcode NM00012023CTU was confirmed and preserved at National Plant Resources Center - Vietnam. To maintain sample integrity, they were promptly frozen for future analysis.

Extraction and isolation of anticancer compounds

The entire NM underwent drying at 55 °C to remove moisture. The plant material was fragmented into smaller pieces, and a grinding process was performed using a Waring laboratory blender (Cole-Parmer, USA). This process resulted in a final moisture content of 8.85 ± 0.47%. To ensure preservation and stability, the sample was carefully stored in a sealed plastic bag and kept at −20 °C for further extraction. For the extraction procedure, the samples were immersed in methanol (Merck, Germany) and subjected to 3 consecutive 24 h soaking cycles. Subsequently, all supernatants were combined, filtered to remove particulate matter, and concentrated by rotary evaporation (BUCHI Rotavapor R300, Flawil, Switzerland), yielding a crude extract at 24.28% (**Table S2**). Fractionation in ascending order of polarity solvents yielded 3 fractions: *n*-hexane extract (NMHex, 101 g), ethyl acetate extract (NMEtOAc, 223 g), and aqueous extract.

Subsequently, NMHex was purified by column chromatography on silica gel 60 with particle sizes ranging from 230 to 400 mesh (ASTM, Sigma-Aldrich, USA). Seven sub-fractions (denoted as H.1 to H.7) were obtained with a gradient elution according to polarity from n-hexane, ethyl acetate, and methanol, respectively. Sub-fraction H.4 underwent further purification following the ratios of n-hexane and chloroform (Hex:TCM, 100:00 to 0:100, *v/v*), ultimately yielding compound **1** (14 mg). Similarly, NMEtOAc was processed according to the same procedure above, resulting in 7 sub-fractions labeled E.1 to E.7. Additionally, a series of solvent gradients was carried out, including n-hexane and chloroform (Hex: TCM, 100:0 to 0:100, *v/v*), n-hexane and dichloromethane (Hex: DCM, 100:0 to 0:100, *v/v*), or chloroform-methanol (TCM: MeOH, 93:7, v/v), which resulted in the isolation of compound **2** (12 mg), compound **3** (185 mg), and compound **4** (155 mg). The purification process was conducted using thin-layer chromatography (TLC) on pre-coated silica gel plates, indicated by fluorescent F-$_{254}$ (Silica gel 60 F-$_{254}$, Merck, Germany). Spot detection was visualized under UV light (254 and 365 nm) and by color changes resulting from spraying with 5% vanillin/H_2SO_4 (*v/v*) in ethanol and heating on a hot plate, respectively.

Cell culture and cell cytotoxicity

HeLa (CCL-2^{TM}) and HEK293 (CRL-1573^{TM}) were obtained from the American Type Culture Collection (ATCC, Manassas, VA, USA). Cells were cultured with Dulbecco's Modified Eagle's Medium (DMEM; GIBCO, Thermo Fisher Scientific, USA) supplemented with 10% fetal bovine serum (FBS; Hyclone, USA), 2mM L-glutamine, and 1% penicillin-streptomycin (Merck, Germany). The cultures were maintained in humidified incubators with 5% CO_2 atmosphere at 37 °C.

For the cytotoxicity assay, approximately 1×10^4 cells/mL were seeded in 96-well plates and incubated for 24 or 48 h. In short, cells were subsequently treated with various concentrations of the extract, diluted in a mixture of dimethyl sulfoxide and DMEM, with a final DMSO concentration of 0.1% (*v/v*). After removing the old media, cell culture medium was replaced with a mixture of 10 µL CCK-8 Kit (CCK-8; Dojindo Molecular Technologies Inc., Rockville, USA) and 90 µL DMEM, according to the manufacturer's instructions. Finally, the optical density was measured at 450 nm by a microplate reader (Epoch, BioTek, USA). Ellipticine, a tetracyclic alkaloid used for cancer treatment, served as a positive control (Sigma-Aldrich, USA).

Selectivity index

For potential assessment of samples, the selectivity index (S.I.) was defined as the concentration ratios of 50% inhibitory concentration (CC_{50}) in non-cancerous cells to that in cancer cells (IC_{50}) as expressed by the following formula below [14]:

$$SI = \frac{CC_{50\,(non-cancerous\,cell)}}{IC_{50(cancer\,cell)}}$$

Colony formation assay

For the clonogenic assessment, cells (approximately 5×10^2 cells/well) were placed in 12-well plates for 24 h. Then, the designated sample doses were added over 24 or 48 h. After sample incubation, the culture medium was replaced every 2 days, and the cells were incubated for an additional 10 days to allow for colony formation. Then, the cells were washed twice with phosphate-buffered saline (PBS), fixed with 4% paraformaldehyde (PFA) for 10 min, and then stained with 0.5% crystal violet for 30 min. Finally, colony formation was visualized using a digital microscope (Olympus CKX53SF, Tokyo, Japan) with the LCmicro 2.2 application and quantified using ImageJ software (National Institutes of Health, USA).

Scratch wound-healing migration assay

Cells were plated as a singular layer in 24-well plates and incubated for 24 h under the conditions described above. After 24 h of starvation, a scratch wound was created to disrupt the cell monolayer using a 200 µL pipette tip. 20 µM of Mitomycin C (FUJIFILM Wako, Tokyo, Japan) was added prior to scratching and sample application for 2 h in basal DMEM medium to inhibit proliferation. Wound closure due to cell migration was examined microscopically at 0, 24, and 48 h, respectively. Data was analyzed using ImageJ and presented as a percentage of wound area closure at 24 and 48 h relative to the initial wound area (0 h) [15].

Intracellular ROS assessment

Intracellular ROS levels were measured using the Cellular ROS Assay Kit (Abcam, Tokyo, Japan) according to the manufacturer's instructions. Cells were washed with PBS and stained with 2',7'-dichlorodihydrofluorescein diacetate ($DCFH_2$ –DA) at a final concentration of 10 μM for 45 min in an incubator at 37 °C. The fluorescence intensity was determined using a Wallac 1420 spectrofluorometer (Perkin-Elmer, Turku, Finland).

Real-time quantitative reverse transcription PCR

For this assessment, cells were seeded in 6-well plates under the same conditions as described above and subsequently incubated with the samples. After that, RNA extraction was performed using the Trizol reagent (FUJIFILM Wako, Tokyo, Japan) and the Qiagen RNeasy Kit (Qiagen, Germany), following the manufacturer's instructions. RNA concentrations were quantified with a NanoDrop microvolume spectrophotometer (Thermo Scientific, USA). Complementary DNA (cDNA) synthesis was followed using Transcriptor Universal cDNA Master (Roche, Tokyo, Japan). Finally, the gene expression was evaluated using RT-*q*PCR as described in our previous report [16]. *β-actin* served as a normalization control. All primer sequences were confirmed using Primer-BLAST (NCBI, NIH, USA) and are presented in the Supplementary Materials (**Table S1**).

Western blotting

Western blotting was essentially performed as described previously to evaluate the effect of the compound [17]. The control and sample were harvested, washed with PBS, and subsequently lysed in RIPA buffer (FUJIFILM-Wako, Japan) containing phosphatase/protease inhibitor. Afterward, the BCA protein assay (Thermo Fisher Scientific, USA) was used to determine the protein concentration in cell lysates. Next, samples were subjected to SDS-polyacrylamide gel electrophoresis (SDS-PAGE, 10%, (v/v)) and then blotted onto Immobilon PVDF membrane (Merck Life Sciences, USA). The membrane was blocked with OneStep Blocker (Bio-Helix, Taiwan) for 1 h at room temperature, then incubated overnight at 4 °C separately with rabbit-derived primary antibodies (dilution 1:1000) against cleaved caspase-3, Bax, Bcl-2, and GAPDH (Cell Signaling Technology, USA). After washing with TBST, the membranes were incubated with the appropriate horseradish peroxidase (HRP)-conjugated secondary antibodies (1:2000) for 1 h at room temperature. The blots were exposed to SuperSignal West Atto Ultimate sensitivity substrate (Thermo Fisher Scientific, USA) to visualize the immunostained polypeptides. Band intensities were quantified using ImageJ software (National Institutes of Health -NIH, MD, USA). The expression levels of cleaved caspase-3, Bax, and Bcl-2 were normalized to GAPDH.

Apoptosis detection assay

Apoptosis was assessed using an Annexin V-FITC/Propidium iodide (PI) Apoptosis Detection Kit (#640914, BioLegend, USA) according to the manufacturer's instructions. Cells (density of 2×10 ^5 cells/well) were seeded in 6-well plates overnight, then treated with compounds at 25 and 50 μM for 24 h before harvesting. Cells were trypsinized, washed with Staining Buffer (Biolegend, USA), and resuspended in kit-provided Binding Buffer. After staining with Annexin V and propidium iodide solution for 15 min at 25 °C, cells were analyzed by the RF-500 flow cytometer (Sysmex, Hyogo, Japan).

General procedure for structure elucidation

Chemical structures were analyzed using a Bruker Avance III-600 MHz spectrometer (Bruker, Rheinstetten, Germany) with $CDCl_3$, CD_3OD and DMSO-d_6 as appropriate.

Statistical analysis

Results are presented as the mean ± standard deviation (S. D.) of at least 3 independent replications. One-way ANOVA was used to determine statistical significance between groups ($p < 0.05$), followed by Tukey's post-hoc test using GraphPad Prism software version 10.0.1 (GraphPad Software Inc., CA, USA).

Results and discussion

Effects of *Nepenthes mirabilis* methanol extract against HeLa cervical cancer cells

The CCK-8 assay was employed to evaluate the anti-proliferative activity of the *N. mirabilis* (NM) extract and its sub-fractions against the HeLa human

cervical cancer cell line, with non-cancerous cells used as a parallel control. Consistent with our previous findings, the NM methanol extract exhibited a selectivity index (S. I.) greater than 1.0, indicating a preferential cytotoxic effect on cancer cells over non-cancerous cells [11]. Additionally, NM extract did not affect another cervical cell line (C33A) or other cell lines (e.g, HT-29, a colon cancer cell line, or HepG2, a hepatic cell line) [11]. This suggested the potential activity of NM or its active ingredients, as well as selectivity towards cervical cancer cell lines. It should be noted that these primary observations do not conclude whether the anti-proliferative activity of *Nepenthes mirabilis* is equal across different stages of cervical cancer. Cervical cancer's biological heterogeneity, varying with clinical stage, histological subtype, HPV status, and molecular alterations, suggests that the findings may not apply uniformly across all stages. Therefore, this evidence is model-specific, and further research with diverse cervical cancer models is needed to ascertain stage- or subtype-dependent sensitivity. Here, the primary focus of this study was to evaluate the effects of NM extract and, more specifically, to identify the components responsible for the observed positive outcomes, thereby paving the way for potential therapeutic applications.

Table 1 Cytotoxicity of *Nepenthes mirabilis* methanol extract on HeLa and HEK293 cell lines.

Sample	Cytotoxicity		Selectivity Index (S. I.)	Harvest time	Ref.
	HeLa cell IC_{50} (µg/mL)	HEK293 cell CC_{50} (µg/mL)			
Nepenthes mirabilis methanol extract	151.35 ± 41.58	281.84 ± 2.35	1.86	June 2024	[11]
	59.33 ± 4.04	226.60 ± 1.53	3.82	January 2023	-

Table 1 compares the cytotoxicity and selectivity of *N. mirabilis* methanol extracts collected at different harvesting times, illustrating potential variation in biological activity associated with harvesting conditions. In the present study, the result illustrated that the IC_{50} value of NM extract was determined to be 59.33 µg/mL and considerably enhanced cytotoxicity on HeLa cancer cells in comparison with our previous result (IC_{50}, 151.35 µg/mL), whereas an IC_{50} value of 226.60 µg/mL was observed on HEK293, human embryonic kidney cells. This value indicated that the NM extract exhibited considerable selectivity toward HeLa cells relative to HEK293 cells, meaning it is significantly more toxic to cancer cells than to non-cancerous cells. The lower IC_{50} value indicated a significant improvement in its ability to target and kill cancer cells compared to previous observations. Additionally, the comparatively high IC_{50} value against HEK293, coupled with an SI of 3.82 for the accepted toxicity threshold, further reinforces the potential of the NM extract as selective toward HeLa cells relative to HEK293 cells (**Table 1**). These results indicated that NM extract exhibited moderate anti-proliferative activity, as reflected by an IC_{50} value within 50 - 200 µg/mL, in agreement with a previous study [12]. Notably, the difference points indicate that the bioactive ingredients depend on harvest time, meaning that environmental conditions or essential nutrient sources specific to the carnivorous plant species influence the chemical and biological composition of the plant, thereby modifying the synthesis and biological activity of its organic compounds [18,19]. This pointed out that these initial observations could be further explored for specific applications governed by nutrient availability or environmental factors.

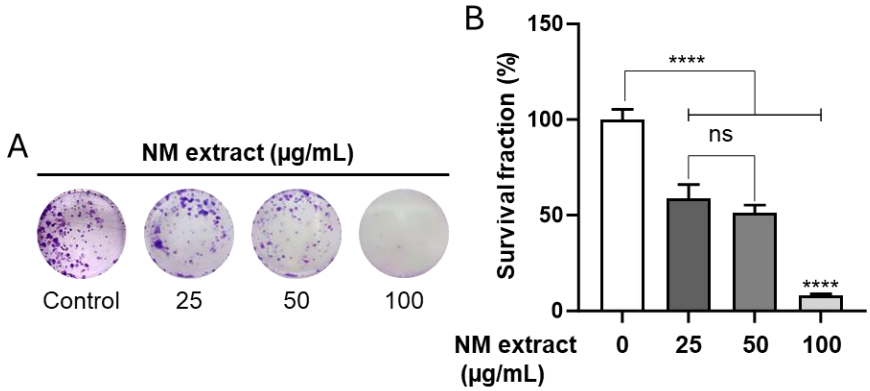


Figure 1 *Nepenthes mirabilis* methanol extract impaired the clonogenic capacity of HeLa cells for 24 h. (A). Survival fraction was quantified by ImageJ; (B). The representation of the number and size of the colonies was analyzed. Data are represented as mean ± S. D (n = 3); ****, $p < 0.0001$ vs control group; ns, not significant.

To evaluate HeLa cell survival after incubation with NM extract, a clonogenic assay was performed. As shown in **Figure 1(A)**, NM extract significantly decreased the number of larger colonies compared to the control group, although no differences were observed between 25 and 50 µg/mL. Notably, the survival fraction was approximately 8.12% at 100 µg/mL, indicating impairment of clonogenic survival in HeLa cells (**Figure 1(B)**). Similarly, wound coverage was eventually closed after 48 h in the experimental group, compared with the control group at 0 h, while a significant gap persisted in the NM extract-treated group during the investigated time (**Figure 2(A)**). For instance, the analyzed results indicated that the percentage of wound closure decreased dramatically to 73.1% and 32.47% at 25 and 50 µg/mL of NM extract, respectively, after 24 h. However, there was no significant difference between 24 and 48 h in the NM extract concentration of 50 µg/mL (**Figure 2(B)**). This observation demonstrated the anti-migratory effect of the NM extract on HeLa cells in a dose-dependent manner. Colony formation and cell migration are crucial processes that illustrate the proliferation, invasion, and metastasis of cancer cells, enabling them to exert their biological functions [14]. Thus, these results suggest the NM extract suppresses clonogenic growth and migratory capacity of HeLa cells.

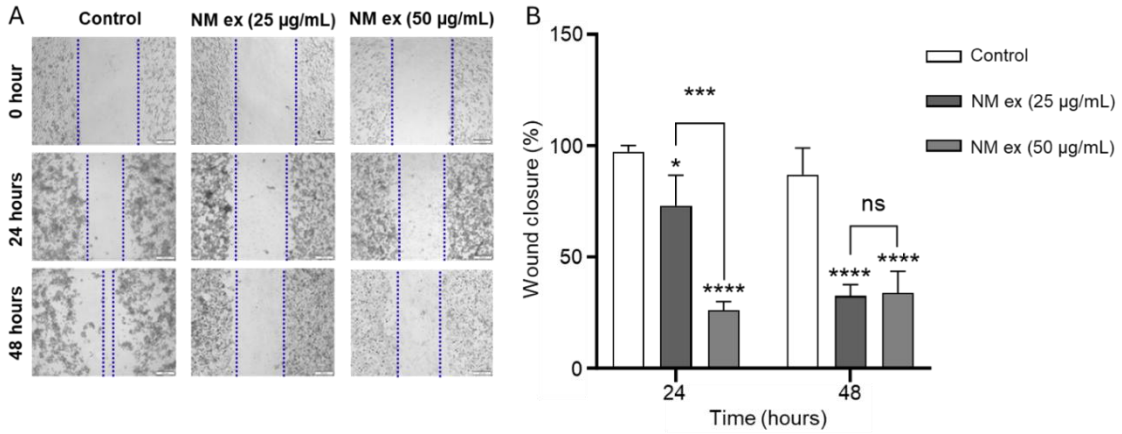


Figure 2 *Nepenthes mirabilis* methanol extract significantly suppressed HeLa cell migration at 24 and 48 h. (A) Representatives of migratory cells were observed under an inverted microscope; (B) Wound closure rates of NM extract compared to control group were quantitatively analyzed by Image J. Data are represented as mean ± S.D. (n = 3); *$p <$ 0.05; ***$p < 0.001$; ****$p < 0.0001$ *vs* control group; ns, not significant.

Nutrient deprivation triggers the production of mitochondria-derived reactive oxygen species, which induce autophagy, destabilize mitochondria, and promote apoptosis [20,21]. As shown in **Figure 3(A)**, the presence of NM extract significantly increased ROS levels compared to the control group, yielding 1.6- and 2.1-fold increases, respectively. Moreover, the effect of NM extract-induced cytotoxicity via ROS generation was confirmed by co-treatment with N-acetyl-L-cysteine (NAC). Most evidence suggests that NAC, an antioxidant agent, directly attenuates ROS production, thereby protecting cells from oxidative damage and apoptosis [22,23]. Here, 50 μg/mL of NM extract induced cell death via intracellular ROS accumulation, whereas co-treatment with NAC enhanced cell survival (**Figure 3(B)**). Therefore, these results imply that NM extract may cause cell death through ROS-mediated apoptosis.

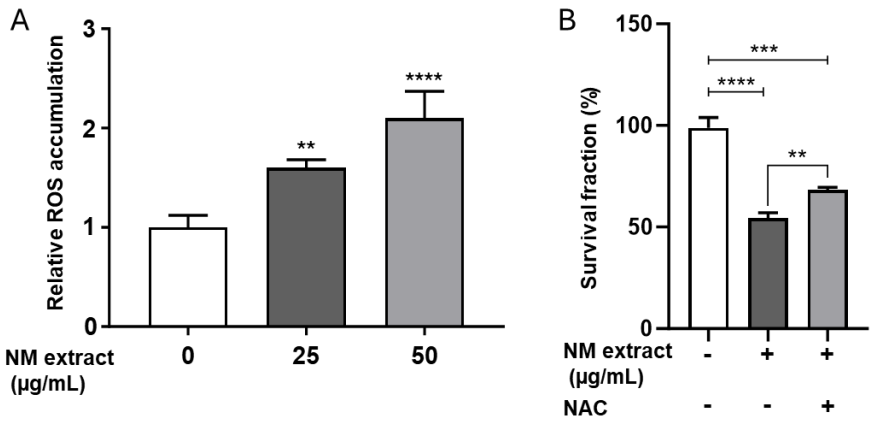


Figure 3 *Nepenthes mirabilis* methanol extract enhanced cell death via ROS-mediated apoptosis. (A) Intracellular ROS accumulation was analyzed by staining with $DCFH_2$–DA on HeLa cells for 24 h; (B) Cell survival rate of NM extract-treated (50 μg/mL) was quantitatively measured using CCK-8 Kit in the presence or absence of NAC (5 mM) for 24 h. Data are represented as mean ± S.D. (n = 4); $^{**}p < 0.01$; $^{***}p < 0.001$; $^{****}p < 0.0001$ vs control group or treatment group.

The PI3K/Akt/mTOR signaling pathway plays a fundamental role in the molecular mechanisms of numerous cancer cells, influencing cell growth, survival, proliferation, and metabolism [24]. In particular, previous evidence indicated that PI3K activation leads to Akt phosphorylation, resulting in the regulation of cell proliferation and thereby promoting tumor growth [25,26]. Therefore, a potential drug-like agent that inhibits Akt phosphorylation or downregulates Akt kinase activity to suppress cancer cell progression via PI3K/Akt pathway regulation could be developed as an anticancer therapeutic. Besides, Bcl-2 functions as a key downstream effector of the Akt signaling pathway and serves as a potential inhibitor of apoptosis [26]. As an anti-apoptotic protein, Bcl-2 is often upregulated in cancer cells to evade cell death by binding to pro-apoptotic proteins, thereby inhibiting mitochondrial outer membrane permeabilization and blocking cytochrome c release [26,27]. Notably, most anticancer drugs were modified or developed to target Bcl-2, achieving success in early-stage clinical trials [28]. Here, as illustrated in **Figures 4(A) - 4(B)**, the NM extract markedly suppressed mRNA expression of Akt and Bcl-2 compared to the control group. Consequently, NM extract inhibited the proliferation and migration of cervical cancer cells while promoting apoptosis, potentially by regulating the PI3K/Akt signaling axis. These primary findings also suggest the potential presence of bioactive compounds that inhibit HeLa cells, warranting further exploration.

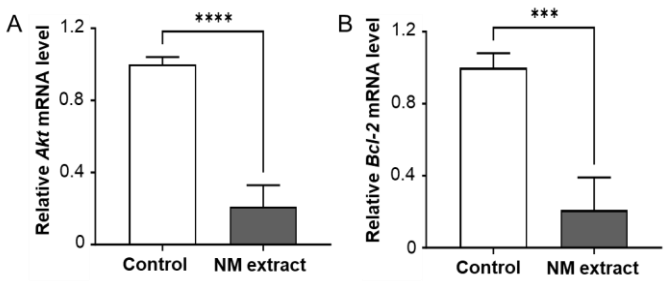


Figure 4 Relative gene-targeted expression analysis under treatment of *Nepenthes mirabilis* methanol extract on HeLa cells. (A). mRNA *Akt* expression level was analyzed on 50 µg/mL of NM extract; (B). mRNA *Bcl-2* expression level was analyzed on 50 µg/mL of NM extract. Data are represented as mean ± S.D. (n = 4); ***, $p < 0.001$; ****, $p < 0.0001$ vs control group.

For this reason, the fractions of NM extract were evaluated for their anti-proliferative activity at a fixed concentration against HeLa cervical cancer cells, typically 50 µg/mL. The results indicated that NMEtOAc significantly reduced cell survival, resulting in approximately 56% reduction in cell viability. Notably, NMHex showed a survival rate of approximately 61%, whereas no significant difference was observed in the aqueous extract (data not shown). Contrary to typical observations, it is noted that active ingredients are concentrated in the moderately polar fraction. In this case, the anticancer components were more broadly distributed, including in the non-polar fraction, consistent with a previous study [29]. Thus, NMEtOAc and NMHex were selected to explore potential anti-HeLa agents for cervical cancer.

Effect of active ingredients from NM extract on HeLa Cervical cancer cells

To ascertain the distinct active constituents present within NMEtOAc and NMHex extracts, classical column chromatography was applied, and 4 compounds were isolated. Each sample's activity was initially assessed at a fixed concentration based on its toxicity to HeLa cells. As depicted in Figure 5A, the presence of these compounds slightly suppressed the cell viability, except for compound **4**. Remarkably, compound **1** dramatically enhanced cell death compared to the control, reaching approximately 48%. Similarly, ellipticine exhibited anti-proliferative effects, reducing HeLa cell viability by roughly 54% at 2 µg/mL [30]. Moreover, intracellular ROS levels increased following exposure to compounds **1**, **2**, and **3**, whereas compound **4** had no significant effect (**Figure 5(B)**). These findings imply that the presence of active compounds may promote oxidative stress, which could contribute to subsequent apoptotic cell death.

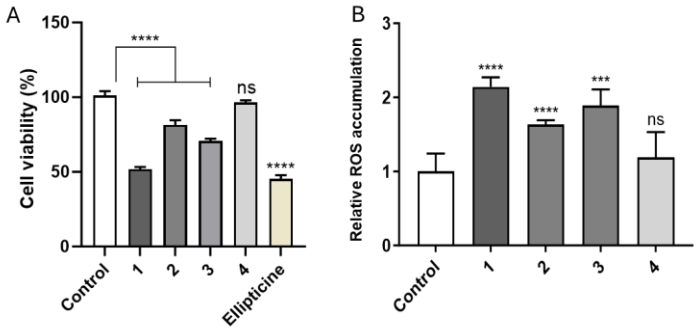


Figure 5 Anti-proliferative effect of active ingredients from *Nepenthes mirabilis* methanol extract on HeLa cells. (A). Cell viability was assessed using CCK-8 Kit with 10 µg/mL of each compound or 2 µg/mL of Ellipticine for 24 h; (B). $DCFH_2$-DA staining was used to assess intracellular ROS accumulation with 10 µg/mL of each compound for 24 h. Data are represented as mean ± S.D. (n = 4); ***$p < 0.001$; ****$p < 0.0001$ vs control group; ns, not significant.

To further elucidate the structures and identities of all isolated ingredients, 1D and 2D NMR analyses were performed and compared with our previous study and the present literature (Supplementary Materials). As illustrated in **Figure 6**, 4 compounds were initially identified, including nepenthone C (**1**), quercetin (**2**), gallic acid (**3**), and daucosterol (**4**). Remarkably, even compounds **3** and **4** were commonly encountered; however, they were first isolated and purified from this species.

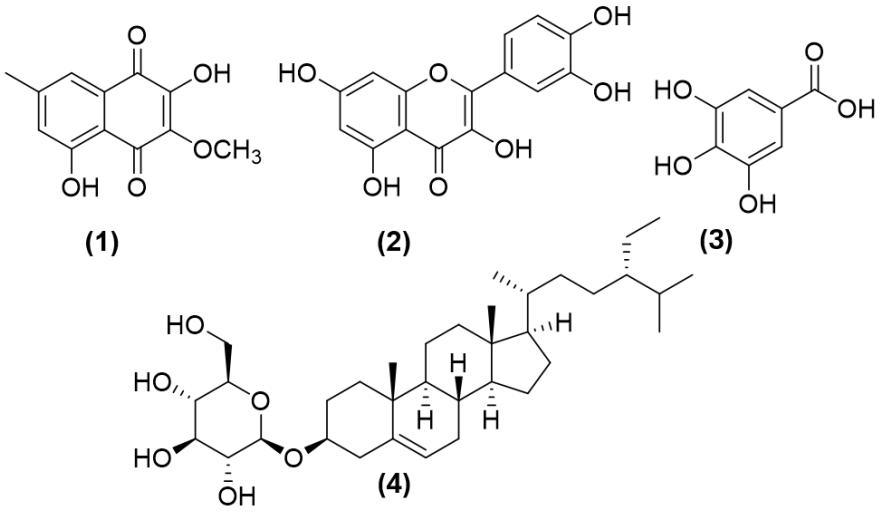


Figure 6 Structures of 4 active compounds isolated from *Nepenthes mirabilis* methanol extract.

To confirm the anticancer efficacy of these compounds, the cytotoxicity-related IC_{50} values were subsequently evaluated and summarized in Table 2. Here, nepenthone C and quercetin, numbered as compounds 1 and 2, respectively, exhibited the greatest toxicity against HeLa cells, with IC_{50} values of 43.54 and 180.1 µM, respectively, compared with other compounds. In contrast, gallic acid exhibited lower activity, with an IC_{50} greater than 200 µM. A previous study reported that gallic acid inhibited the growth of HeLa cells, with an approximate IC_{50} value of 80 µM at 24 h [31]. Moreover, an IC_{50} of around 58 µM after 72 h was observed, suggesting that the toxicity increased significantly with exposure time [32]. A recent study reported similar values of 379.3 and 239.2 µM after 24 and 48 h of treatment, respectively, consistent with our observations [33]. This can be explained by the differences in cell densities and experimental conditions. Indeed, most evidence indicates that gallic acid induces cell death via apoptosis and/or necrosis, leading to ROS release and GSH depletion [34,35]. Another finding, in combination with gallic acid and doxorubicin, significantly enhanced the efficiency of apoptosis associated with p53/Bax differences. Thus, this data suggests a promising therapeutic alternative approach to chemotherapy agents [33]. Unfortunately, despite similar published results, the weak cytotoxicity of daucosterol observed in HeLa cells did not align with the previously reported selectivity against other cancer cell lines [36]. In accordance with the above result, quercetin showed moderate effectiveness and selectivity, with an IC_{50} of 180.1 µM (SI, 1.06). This data was less effective than previous evaluations, which showed IC_{50} values of 125 and approximately 97.64 µM (29.49 µg/mL), respectively [37,38]. As expected, some evidence indicates that quercetin, a dietary compound, induces apoptosis in cervical cancer cells, depending on the cell cycle, via upregulation of the NF-κB and/or PI3K/Akt signaling pathways [39,40]. In particular, nepenthone C showed the greatest cytotoxicity against cervical cancer cells (IC_{50}, 43.54 µM; SI, 6.44), demonstrating both anti-proliferative and selective effects.

Table 2 Cytotoxicity of isolated compounds on HeLa and HEK293 cell lines.

Compound	Name	Cytotoxicity		Selectivity Index (S.I.)
		HeLa cell IC_{50} (µM)	HEK293 cell CC_{50} (µM)	
1	Nepenthone C	43.54 ± 2.58	280.3 ± 3.72	6.44
2	Quercetin	180.1 ± 3.41	191.3 ± 1.39	1.06
3	Gallic acid	>200	67.3 ± 2.11	-
4	Daucosterol	>200	>200	-

"-", not applicable.

Moreover, the notable increase in intracellular ROS induced by nepenthone C provided supportive evidence that oxidative stress may play an essential role in mediating its cytotoxicity. These findings suggest that the apoptosis observed in HeLa cells may, at least in part, be attributed to ROS-dependent pathways. Notably, the structure-activity relationship analysis highlights the role of the hydroxyl group. Their presence could enhance or diminish activities, depending on their number, position, and contribution to the compounds' overall polarity [41]. Additionally, bulky or complex substituents often reduce cytotoxicity, especially when they cause steric hindrance or disrupt the balance between lipophilicity and hydrophilicity (e.g., daucosterol) [39,40]. These findings provide evidence that nepenthone C, a naphthoquinone derivative, induces ROS-mediated apoptosis in cervical cancer cells. Following the identification of nepenthone C as the most active compound, subsequent investigations were conducted to explore its underlying mechanisms, particularly its ability to induce apoptosis in HeLa cells.

Mechanism investigation of nepenthone C-induced apoptosis

To further clarify whether nepenthone C (Nep.C)-induced cytotoxicity was associated with apoptotic cell death, Annexin V/PI flow cytometry and Western blot analyses were performed. Flow cytometry revealed a dose-dependent increase in the proportion of apoptotic cells in response to nepenthone C treatment (**Figures 7(A) - 7(B)**). In particular, Nepenthone C treatment at 25 µM slightly increased the apoptotic population to 12.66%. More prominently, 50 µM nepenthone C markedly elevated both early and late apoptotic cells, resulting in a total apoptosis rate of 26.19% compared with the control group. This observation suggested that nepenthone C triggered programmed cell death. Importantly, co-treatment with NAC partially attenuated Nep.C-induced apoptosis (26.19% to 16.76%) and restored cell viability (72.75% to 81.59%), suggesting that intracellular ROS generation contributes, at least in part, to Nep.C-induced apoptosis. Consistently, western blot analysis indicated that nepenthone C treatment markedly increased cleaved caspase-3 expression, significantly down-regulated the anti-apoptotic protein Bcl-2 level, whereas the pro-apoptotic Bax expression showed a modest change (**Figures 8(A) - 8(B)**). Consequently, the Bax/Bcl-2 ratio was elevated, primarily due to decreased Bcl-2 levels. These observations suggested the involvement of the intrinsic mitochondrial apoptotic pathway, although Bax activation might not be a primary regulator (**Figure 8(C)**). Remarkably, co-treatment with NAC tended to reduce these effects, further reinforcing the ROS accumulation acts, at least in part, upstream of Nep.C-induced apoptosis. However, the partial protective effect of NAC suggests that ROS accumulation contributes to nepenthone C-induced apoptosis but does not fully contribute to cell death. Increased cleaved caspase-3, decreased Bcl-2, and an elevated Bax/Bcl-2 ratio point to mitochondrial and caspase-associated apoptotic signaling. Thus, nepenthone C-induced apoptosis may involve both ROS-dependent upstream events and downstream caspase-mediated pathways. This represents a limitation of the present study. Further investigation using caspase-3/7 activity assays, PARP cleavage analysis, mitochondrial membrane potential assessment, and pan-caspase inhibition will be needed to clarify these mechanisms.

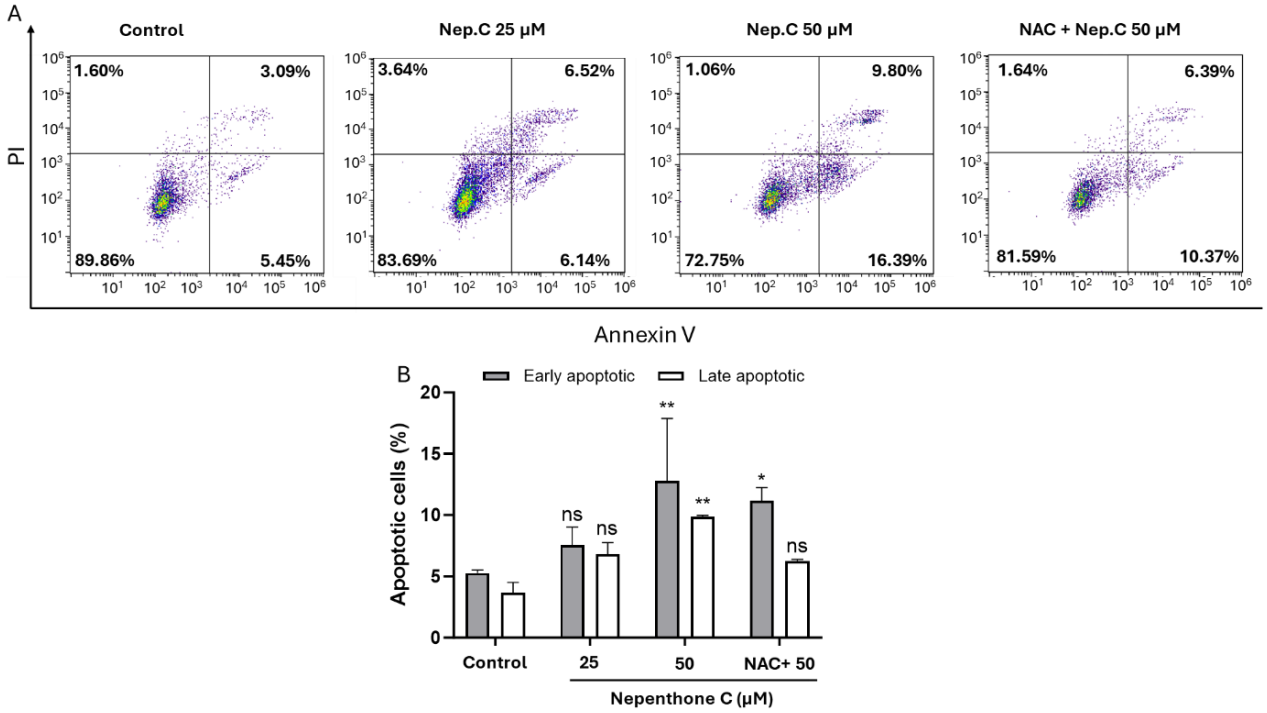


Figure 7 Nepenthone C induced apoptosis in HeLa cells as determined by Annexin V-FITC/PI staining. (A) Representative Annexin V-FITC/PI flow cytometry plots of HeLa cells treated with *nepenthone C* (25 and 50 μM), NAC, and nepenthone C (50 μM) + NAC for 24 h; (B) Percentage of early and late apoptotic cell populations. Data are represented as mean ± S.D. (n = 3); *$p < 0.05$; **$p < 0.01$; ns, not significant.

Consistent with the well-recognized redox-active nature of naphthoquinone derivatives, the mechanism profile suggests that they induce oxidative stress and cell death in cancer cells via redox cycling, ROS accumulation, semiquinone formation, and interactions with thiol-containing proteins [42]. Previous studies have established similar pathways for other naphthoquinones; for instance, plumbagin induces ROS-mediated apoptosis in cervical cancer cells, while shikonin, another potent naphthoquinone, promotes HeLa cell death via caspase-3 activation and inhibition of DNA synthesis [43]. Similarly, juglone induces apoptosis via ROS-mediated mitochondrial damage, activating caspase-dependent pathways [44]. Our findings showed that nepenthone C also increases intracellular ROS, promotes apoptosis, enhances cleaved caspase-3, downregulates Bcl-2, and increases the Bax/Bcl-2 ratio, consistent with these established naphthoquinone mechanisms. One important note is that the 1,4-naphthoquinone core of nepenthone C likely drives its redox cycling and ROS-associated apoptosis. The 1,4-naphthoquinone core is a redox-active pharmacophore that generates reactive oxygen species and oxidative stress-mediated cytotoxicity by accepting 1 or 2 electrons to form semiquinone/hydroquinone intermediates [45,46]. However, the hydroxyl and methoxy substituents in nepenthone C distinguish it from plumbagin and shikonin. These substitutions may influence electron distribution, hydrogen bonding, polarity, and cellular permeability, potentially reducing nonspecific lipophilic cytotoxicity while maintaining pro-apoptotic redox activity [42,46]. This structural balance might explain nepenthone C's selectivity towards HeLa cells relative to HEK293 cells. Direct potency comparisons with plumbagin and shikonin are difficult due to differences in experimental conditions; further comparative studies are needed to clarify whether nepenthone C's substitution pattern offers improved selectivity or a unique mechanism. While sharing a conserved mechanistic framework, nepenthone C may exhibit moderate potency, requiring higher concentrations to achieve similar apoptotic effects. Thus, our findings classify Nep.C within the broader class of anticancer naphthoquinone derivatives that act, particularly through a ROS-associated apoptotic response. Together with its selectivity for

HeLa cells relative to HEK293 cells (IC50, 43.54 μM; SI, 6.44), these results highlight nepenthone C as a promising scaffold for further mechanistic validation and anti-cervical-cancer investigations.

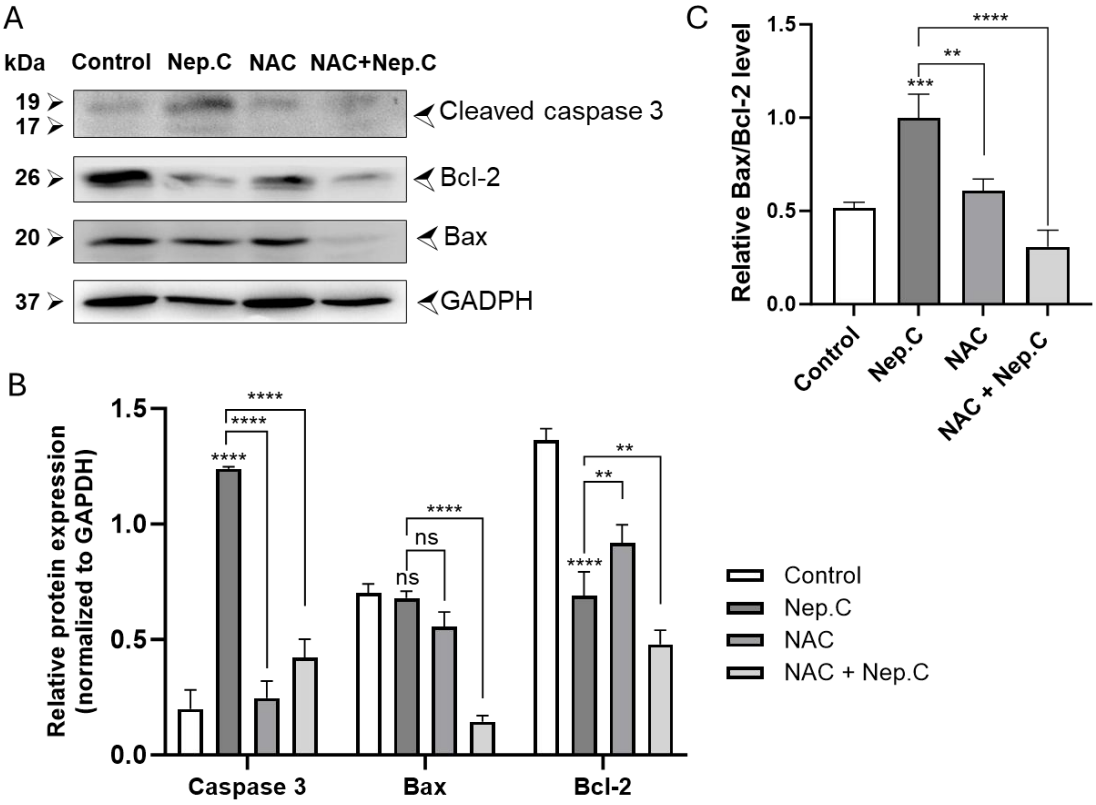


Figure 8 Effect of Nepenthone C on apoptosis-related protein expression in HeLa cells. (A). Representative western blot images showed the expression of cleaved caspase-3, Bax, and Bcl-2 after treatment with nepenthone C (50 μM), NAC, and nepenthone C (50 μM) + NAC for 24 h. GAPDH was taken as a loading control; (B). Quantification of cleaved caspase-3, Bax, and Bcl-2 expression normalized to GAPDH; (C) Bax/Bcl-2 ratio calculated from normalized protein levels. Data are represented as mean ± S.D. (n = 3); $^{**}p < 0.01$; $^{***}p < 0.001$; $^{****}p < 0.0001$; ns, not significant.

Overall, the present results provide the first evidence that nepenthone C exerts its anticancer activity against HeLa cells, at least in part, through ROS-associated mitochondrial apoptosis. Although nepenthone C appears to engage an apoptotic signaling cascade similar to that reported for other anticancer naphthoquinones, further investigations are warranted to understand its selectivity for HeLa cells versus HEK293 cells, identify upstream targets, and assess its therapeutic potential in more advanced experimental models. Besides, it is necessary to confirm whether the anti-proliferative effects of *N. mirabilis* and nepenthone C differ across cervical cancer stages or molecular subtypes.

Conclusions

The present study provides the first mechanistic evidence supporting the anti-cervical cancer potential of *Nepenthes mirabilis* and its major active constituent. Bioactivity-guided isolation identified nepenthone C as the most active compound, exhibiting the greatest selectivity toward HeLa cells compared with HEK293 cells. Mechanistically, nepenthone C induced selective cytotoxicity and apoptosis via ROS-mediated mitochondrial signaling, as evidenced by enhanced caspase-3 activation and an elevated Bax/Bcl-2 ratio. Additionally, NAC's partial attenuation of apoptosis further supports the notion that ROS contribute to upstream nepenthone C-induced cell death. These findings highlight nepenthone C as a potential natural lead compound for further optimization. Taken together, our study provides new insights into the anticancer

potential of *Nepenthes mirabilis* and its constituents. It suggests that nepenthone C is a promising natural naphthoquinone scaffold for further anti-cervical cancer research.

Acknowledgements

The authors gratefully acknowledge the support of the JASSO Follow-up Research Fellowship at Kyoto Institute of Technology, which facilitated research exchange activities relevant to this work.

Declaration of Generative AI in Scientific Writing

Generative AI tools, including ChatGPT (OpenAI), were exclusively used for language and grammar correction. No scientific content or data interpretation was generated by AI; the authors bear full responsibility for the manuscript.

CRediT Author Statement

Thanh Quoc Chau Nguyen: Conceptualization; Methodology; Formal analysis; Software; Writing - Original draft preparation; Funding acquisition. **Tue Minh Duong**: Data curation; Methodology; Software. **Nguyen Trong Tuan**: Visualization; Investigation; Resourse. **Duy Binh Tran**: Visualization. **Tuan Le Anh Pham**: Software; Validation. **Tomonori Waku**: Software. **Kenji Kanaori**: Supervision; Writing - Reviewing and Editing. **Kaeko Kamei:** Supervision; Writing - Reviewing and Editing.

References

[1] NP Thao, BTT Luyen, JE Koo, S Kim, YS Koh, NV Thanh, NX Cuong, PV Kiem, CV Minh and YH Kim. *In vitro* anti-inflammatory components isolated from the carnivorous plant *Nepenthes mirabilis* (Lour.) Rafarin. *Pharmaceutical Biology* 2016; **54(4)**, 588-594.

[2] A Mithöfer. Carnivorous plants and their biotic interactions. *Journal of Plant Interactions* 2022; **17(1)**, 333-343.

[3] MAF Rosli, KA Azizan and HH Goh. Antioxidant activity of pitcher extracts from 3 *Nepenthes* species. *Sains Malaysiana* 2018; **47(12)**, 3069-3075.

[4] MAF Rosli, A Mediani, KA Azizan, SN Baharum and HH Goh. UPLC-TOF-MS/MS-based metabolomics analysis reveals species-specific metabolite compositions in pitchers of *Nepenthes ampullaria*, *Nepenthes rafflesiana*, and their hybrid *Nepenthes* × *hookeriana*. *Frontiers in Plant Science* 2021; **12**, 655004.

[5] NV Quy, LV Cuong, NV Hop, PT Ha and NH Hai. Interspecific association of dominant tree species in an evergreen broadleaved forest in Phu Quoc National Park, Vietnam. *Journal of Forestry Science and Technology* 2023; **8(2)**, 87-96.

[6] DT Nguyen. Exploring the diversity of leaf beetles (Coleoptera:Chrysomelidae) on the islands of Vietnam: A survey of Phu Quoc Island, South of Vietnam. *International Journal of Tropical Insect Science* 2022; **42(5)**, 3525-3539.

[7] KM Lai, YH Huang, Y Lien and CY Huang. Bioactive potential of *Nepenthes miranda* flower extracts: Antidiabetic, anti-skin aging, cytotoxic, and dihydroorotase-inhibitory activities. *Plants* 2025; **14(16)**, 2579.

[8] NV Thanh, NP Thao, PTT Huong, SH Lee, HD Jang, NX Cuong, PV Kiem, YH Kim and CV Minh. Naphthoquinone and flavonoid constituents from the carnivorous plant *Nepenthes mirabilis* and their anti-osteoporotic and antioxidant activities. *Phytochemistry Letters* 2015; **11**, 254-259.

[9] A Bhattacharya, AK Verma, S Rao, SG Momin, P Radhakrishnanand and P Sarkar. Unlocking the phytochemicals in unopened pitcher fluids of *Nepenthes khasiana*–a GC-MS study. *Intelligent Pharmacy* 2024; **2(2)**, 284-290.

[10] TT Hong, VT Khang, NT Tuan and TQC Nguyen. Bioactivity-guided identification of constituents responsible for the anti-oxidative stress effects of *Nepenthes mirabilis*. *Records of Natural Products* 2026; **20(5)**, e26043785.

[11] NQC Thanh, TG Tue, TTD Huynh, VN Thanh, NH Khiem, VT Khang and TT Hong. Study on investigation of the anti-cancer activity of *Nepenthes mirabilis* extract on various human cancer cell line. *Can Tho University Journal of Science* 2025; **61(3)**, 99-107.

[12] SW Kamau, M Jepkorir, G Kipkoech, IJL Lagu, W Kanda, S Kibunja, R Letoluo, S Barmasai, A Wanyoko, V Ruttoh, J Kuria, PG Mwitari, MP Ngugi and SN Nijeru. Antiproliferative activity of *Grewia villosa* ethyl acetate extract on cervical cancer HeLa cell line: Mechanistic insights through network pharmacology and functional

assays approach. *PLoS One* 2025; **20(9)**, e0331649.

[13] WH Talib, I Alsalahat, S Daoud, RF Abutayeh and AI Mahmod. Plant-derived natural products in cancer research: Extraction, mechanism of action, and drug formulation. *Molecules* 2020; **25(22)**, 5319.

[14] OO Olaleye, DH Kim and KA Spriggs. Antiproliferative activities of some selected Nigerian medicinal plants against breast, liver, and cervical cancer cells. *BMC Complementary Medicine and Therapies* 2024; **24(1)**, 1-15.

[15] E Bahar and H Yoon. Modeling and predicting the cell migration properties from scratch wound healing assay on cisplatin-resistant ovarian cancer cell lines using artificial neural network. *Healthcare* 2021; **9(7)**, 911.

[16] TQC Nguyen, TT Hong, VT Khang, YH Thi Nhu, DT Pham, DH Giao, TTT Tu and K Kamei. Anti-inflammatory constituents isolated from *Launaea sarmentosa* against infection by LPS-stimulated macrophages. *Records of Natural Products* 2024; **18(6)**, 663-673.

[17] TQC Nguyen, YDH Nguyen, TD Binh, TLA Pham, K Kanaori, K Kamei, DTX Trang and TT Nguyen. Anti-inflammatory effects of *Lasia spinosa* leaf extract in lipopolysaccharide-induced RAW 264.7 macrophages. *International Journal of Molecular Sciences* 2020; **21(10)**, 1-18.

[18] G Prinsloo and N Nogemane. The effects of season and water availability on chemical composition, secondary metabolites and biological activity in plants. *Phytochemistry Reviews* 2018; **17(4)**, 889-902.

[19] MR Luna-Samano, C Martínez-Peralta, AG Trejo-Loyo and RE Alcalá. Ecological interactions of carnivorous plants: Beyond the relationship with their prey. *Arthropod-Plant Interactions* 2024; **18(2)**, 193-204.

[20] GE Villalpando-Rodriguez and SB Gibson. Reactive oxygen species (ROS) regulates different types of cell death by acting as a rheostat. *Oxidative Medicine and Cellular Longevity* 2021; **2021**, 9912436.

[21] A Ray, S Jena, B Dash, A Sahoo, B Kar, J Patnaik, PC Panda, S Nayak and N Mahapatra. *Hedychium coronarium* extract arrests cell cycle progression, induces apoptosis, and impairs migration and invasion in HeLa cervical cancer cells. *Cancer Management and Research* 2019; **11**, 483-500.

[22] S Guo, NI Burcus, M Scott, Y Jing and I Semenov. The role of reactive oxygen species in the immunity induced by nano-pulse stimulation. *Scientific Reports* 2021; **11(1)**, 1-13.

[23] L Wang, Y Xu, X Zhao, X Zhu, X He, A Sun and G Zhuang. Antagonistic effects of N-acetylcysteine on lead-induced apoptosis and oxidative stress in chicken embryo fibroblast cells. *Heliyon* 2023; **9(11)**, e21847.

[24] X Lin, Y Fang, X Mi, J Fu, S Chen, M Wu and N Jin. Asiatic acid inhibits cervical cancer cell proliferation and migration via PI3K/AKT/mTOR signaling pathway. *Heliyon* 2024; **10(13)**, e34047.

[25] G Ma, Q Dong, F Li, Z Jin, J Pi, W Wu and J Li. Network pharmacology and *in vivo* evidence of the pharmacological mechanism of geniposide in the treatment of atherosclerosis. *BMC Complementary Medicine and Therapies* 2024; **24(1)**, 53.

[26] IJL Lagu, DW Nyamai and SN Njeru. Phytochemical analysis, *in-vitro* and *in-silico* study of antiproliferative activity of ethyl acetate fraction of Launaea cornuta (Hochst. ex Oliv. & Hiern) C. Jeffrey against human cervical cancer cell line. *Frontiers in Pharmacology* 2024; **15**, 1399885.

[27] G Leisching, B Loos, M Botha and AM Engelbrecht. *Bcl-2* confers survival in cisplatin treated cervical cancer cells: Circumventing cisplatin dose-dependent toxicity and resistance. *Journal of Translational Medicine* 2015; **13(1)**, 328.

[28] F Alharbi, E Almanifi and M Ashrafuzzaman. Targeting *BCL-2* family proteins using BH3 mimetic drugs for cancer therapy: A systematic review of randomized clinical trials. *Medicine in Drug Discovery* 2024; **24**, 100199.

[29] IM Adebisi, BC Gomo, A Usman, CJ Ugwah-Oguejiofor, AM Ramadan, TR Giaze, A Hamidu, JY Oyaniyi, M Umar, T Oduola, A Samaila and I Malami. Evaluation of anti-cervical cancer potential of *Caralluma dalzielii*: An *in vitro* approach. *Pharmacological Research - Natural Products* 2025; **9**, 100420.

[30] M Kostić, M Ivanov, T Markovic, SS Babić, L Barros, R Calhelha, M Sokovic and A Ciric. An in

vitro study of the *Origanum minutiflorum* O. Schwarz & P. H. Davis and *Coriandrum sativum* L. essential oils as chronic tonsillitis therapeutics: Antibacterial, antibiofilm, antioxidant, and cytotoxic activities. *Journal of Essential Oil Research* 2022; **34(6)**, 533-543.

[31] BR You, HJ Moon, YH Han and WH Park. Gallic acid inhibits the growth of HeLa cervical cancer cells via apoptosis and/or necrosis. *Food and Chemical Toxicology* 2010; **48(5)**, 1334-1340.

[32] H Abdullah, I Ismail, R Suppian and NM Zakaria. Natural gallic acid and methyl gallate induces apoptosis in HeLa cells through regulation of intrinsic and extrinsic protein expression. *International Journal of Molecular Sciences* 2023; **24(10)**, 8495.

[33] U Sarı, F Zaman, İ Özdemir, Ş Öztürk and MC Tuncer. Galic acid induces HeLa cell lines apoptosis via the P53/Bax signaling pathway. *Biomedicines* 2024; **12(11)**, 2632.

[34] WH Park. Gallic acid induces HeLa cell death via increasing GSH depletion rather than ROS levels. *Oncology Reports* 2017; **37(2)**, 1277-1283.

[35] BR You, SZ Kim, SH Kim and WH Park. Gallic acid-induced lung cancer cell death is accompanied by ROS increase and glutathione depletion. *Molecular and Cellular Biochemistry* 2011; **357(1-2),** 295-303.

[36] MM Quradha, R Khan, A Adhikari, A Rauf, U Rashid, S Bawazeer, YS Al-Awthan, O Bahattab and MS Mubarak. Isolation, biological evaluation, and molecular docking studies of compounds from *Sophora mollis* (Royle) Graham ex Baker. *ACS Omega* 2021; **6(24)**, 15911-15919.

[37] AF Clemente-Soto, E Salas-Vidal, C Milan-Pacheco, JN Sánchez-Carranza, O Peralta-Zaragoza and L González-Maya. Quercetin induces G2 phase arrest and apoptosis with the activation of p53 in an E6 expression-independent manner in HPV-positive human cervical cancer-derived cells. *Molecular Medicine Reports* 2019; **19(3)**, 2097-2106.

[38] K Herni, A Subarnas, A Diantini and Y Iskandar. Cytotoxicity of quercetin and quercetin-3-O-rhamnoside of *Etlingera elatior* (Jack) R.M.Sm. leaves against HeLa cervical cancer cells. *Journal of Applied Pharmaceutical Science* 2021; **11(5)**, 085-090.

[39] RV Priyadarsini, RS Murugan, S Maitreyi, K Ramalingam, D Karunagaran and S Nagini. The flavonoid quercetin induces cell cycle arrest and mitochondria-mediated apoptosis in human cervical cancer (HeLa) cells through p53 induction and NF-κB inhibition. *European Journal of Pharmacology* 2010; **649(1-3)**, 84-91.

[40] T Xiang, Y Fang and SX Wang. Quercetin suppresses HeLa cells by blocking PI3K/Akt pathway. *Journal of Huazhong University of Science and Technology* 2014; **34(5)**, 740-744.

[41] Y Huang, G Li, C Hong, X Zheng, H Yu and Y Zhang. Potential of steroidal alkaloids in cancer: Perspective insight into structure-activity relationships. *Frontiers in Oncology* 2021; **11**, 733369.

[42] MM Rahman, MR Islam, S Akash, S Shohag, L Ahmed, FA Supti, A Rauf, ASM Aljohani, WA Abdulmonem, AA Khalil, R Sharma and M Thiruvengadam. Naphthoquinones and derivatives as potential anticancer agents: An updated review. *Chemico-Biological Interactions* 2022; **368**, 110198.

[43] TG Son, S Camandola, TV Arumugam, RG Cutler, RS Telljohann, MR Mughal, TA Moore, W Luo, QS Yu, DA Johnson, JA Johnson, NH Greig and MP Mattson. Plumbagin, a novel *Nrf2/ARE* activator, protects against cerebral ischemia. *Journal of Neurochemistry* 2010; **112(5)**, 1316-1326.

[44] YB Ji, ZY Qu and X Zou. Juglone-induced apoptosis in human gastric cancer SGC-7901 cells via the mitochondrial pathway. *Experimental and Toxicologic Pathology* 2011; **63(1-2)**, 69-78.

[45] CE Pereyra, RF Dantas, SB Ferreira, LP Gomes and FP Silva. The diverse mechanisms and anticancer potential of naphthoquinones. *Cancer Cell International* 2019; **19(1)**, 207.

[46] G Navarro-Tovar, S Vega-Rodríguez, E Leyva, S Loredo-Carrillo, D de Loera and LI López-López. The relevance and insights on 1,4-naphthoquinones as antimicrobial and antitumoral molecules: A systematic review. *Pharmaceuticals* 2023; **16(4)**, 496.

Supplementary Materials

Table S1 List of primers and primer sequences.

No.	Gene name	Primer probes	Sequence
1	*Akt*	Forward	5′- TCCTTGCTTTCAGGGCTGCT -3′
		Reverse	5′- GCCACACGATACCGGCAAAG -3′
2	*Bcl-2*	Forward	5′- GGCCTCAGGGAACAGAATGAT -3′
		Reverse	5′- TCCTGTTGCTTTCGTTTCTTTC -3′
3	*β-actin*	Forward	5′- GGAGGGGGTTGAGGTGTT-3′
		Reverse	5′- GTGTGCACTTTTATTGGTCTCAA-3′

Akt, protein kinase B; Bcl-2, protein kinase B-2.

Table S2 Extraction and solvent fractionation yield of *Nepenthes mirabilis* methanol extract.

Sample	Abbreviation	Mass obtained (g)	Yield (%)
Dried plant powder	-	7000	-
Methanol crude extract	NM crude extract	1700	24.28
n-hexane extract	NMHex	101	5.94
Ethyl acetate extract	NMEtOAc	223	13.12
Aqueous extract	-	-	-

Supplementary spectroscopic data of compound 1

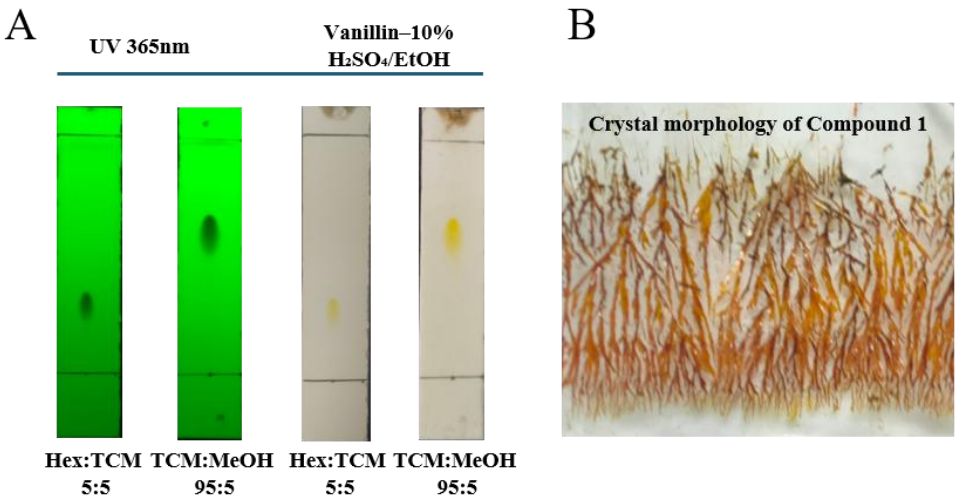


Figure S1 Crystal morphology and TLC profile of compound 1 assigned as nepenthone C. (A). TLC profile of compound 1 on silica gel 60 F_{254}; (B). Dark-red needle-like crystals of compound 1. The plate was visualized with vanillin - 10% H_2SO_4 reagent in ethanol, followed by heating. Compound 1 showed a single yellow spot, suggesting preliminary chromatographic homogeneity.

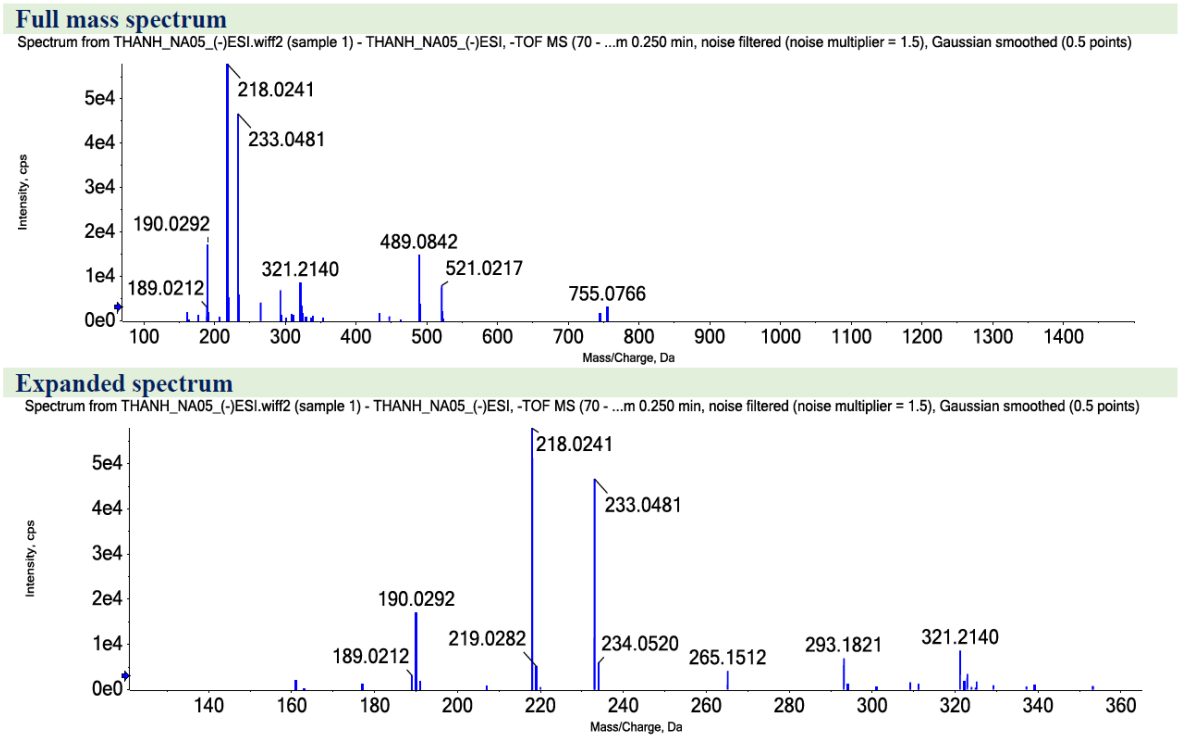


Figure S2 HR-ESI-MS spectrum of compound 1 assigned as nepenthone C in negative ion mode.

Note: The spectrum showed a major ion at m/z 233.0481, corresponding to the deprotonated molecular ion $[M-H]^-$ of nepenthone C ($C_{12}H_{10}O_5$; calculated m/z 233.0455 for $C_{12}H_9O_5^-$).

Table S3 The comparison of the NMR data of compound 1 with a similar compound (Nepenthone C)

Position	Compound 1 ($CDCl_3$)[1]		Nepenthone C ($CDCl_3$) [2]
	^{1}H-NMR (600 MHz) δ_H ppm	^{13}C-NMR (150 MHz) δ_C ppm	^{1}H-NMR (500 MHz) δ_H ppm
1	-	181.7	-
2	-	142.7	-
3	-	139.7	-
4	-	186.3	-
4a	-	110.9	-
5	-	161.8	-
6	7.05 (1H, s)	125.6	7.03 (1H, s)
7	-	147.4	-
8	7.44 (1H, s)	120.7	7.41 (1H, brs)
8a	-	128.9	-
9	4.18 (3H, s)	60.7	4.15 (3H, s)
10	2.40 (3H, s)	21.9	2.38 (3H, s)
5-OH	11.95 (1H, s)	-	11.88 (1H, s)

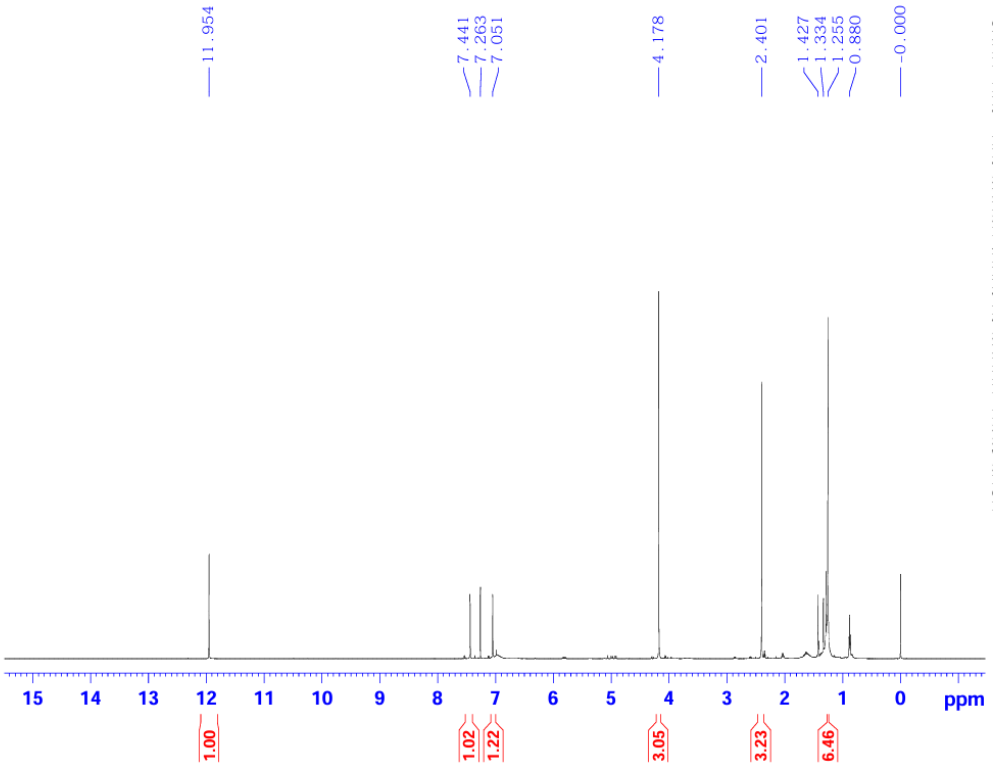


Figure S3 ^{1}H-NMR (600 MHz, $CDCl_3$) spectrum of compound 1 (Nepenthone C). The proton signals were consistent with the reported spectroscopic data of nepenthone C and supported the assignment of compound 1 as a naphthoquinone derivative.

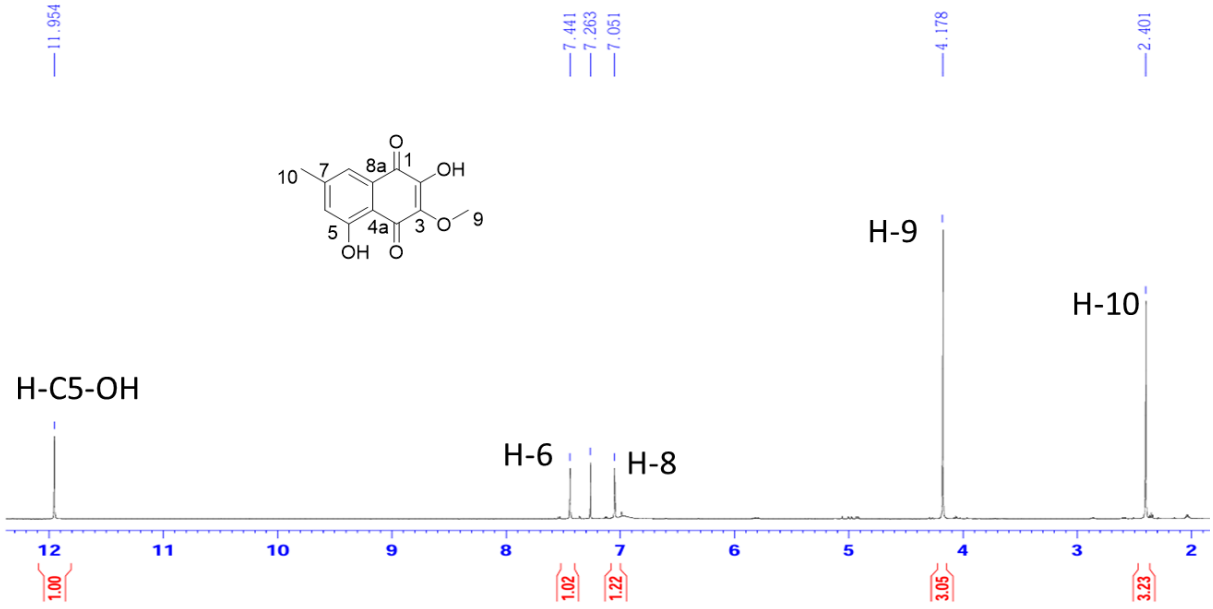


Figure S4 Expanded ^{1}H-NMR (600 MHz, $CDCl_3$) spectrum of compound 1 (Nepenthone C) (from δ_H 2 ppm to δ_H 12.5 ppm). This spectrum highlights the characteristic aromatic, methoxy, methyl, and phenolic hydroxyl proton signals of compound 1. These diagnostic signals were used for comparison with reported nepenthone C data.

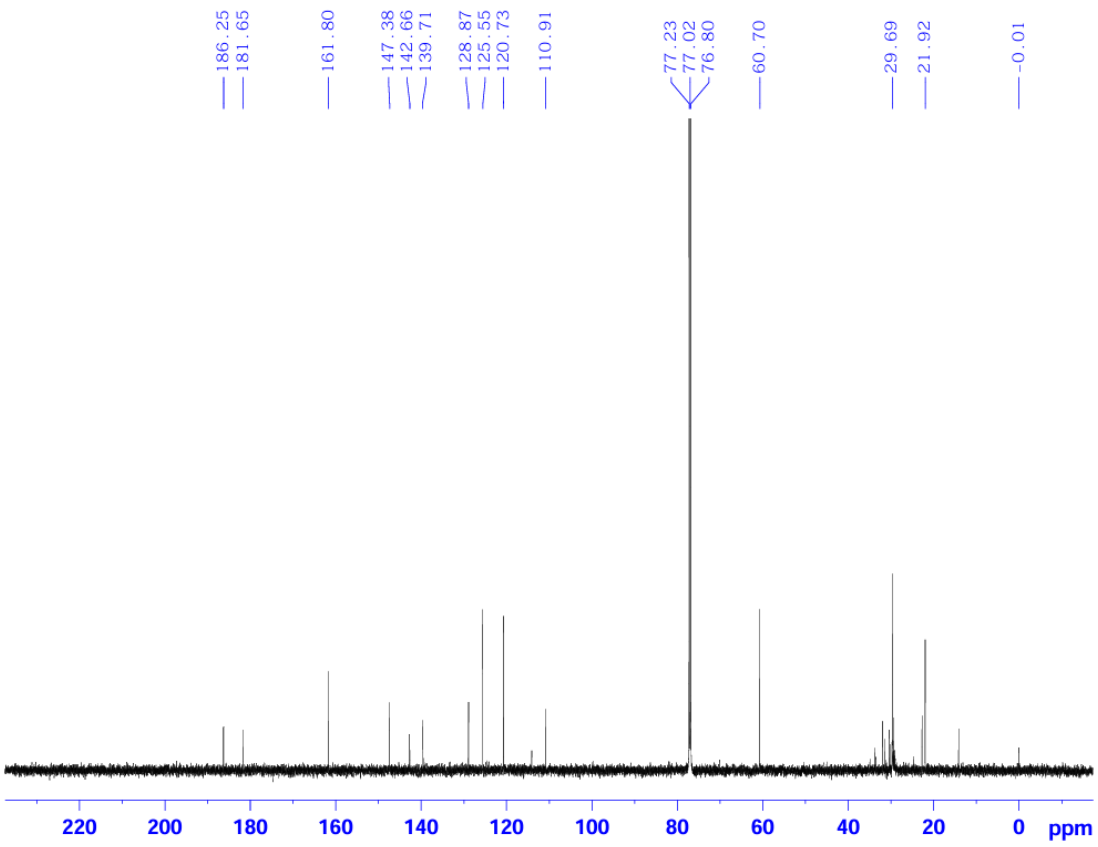


Figure S5 ^{13}C-NMR (150 MHz, $CDCl_3$) spectrum of compound 1 (Nepenthone C). The observed carbon resonances, including quinone carbonyl, aromatic, methoxy, and methyl carbons, support the naphthoquinone skeleton of compound 1.

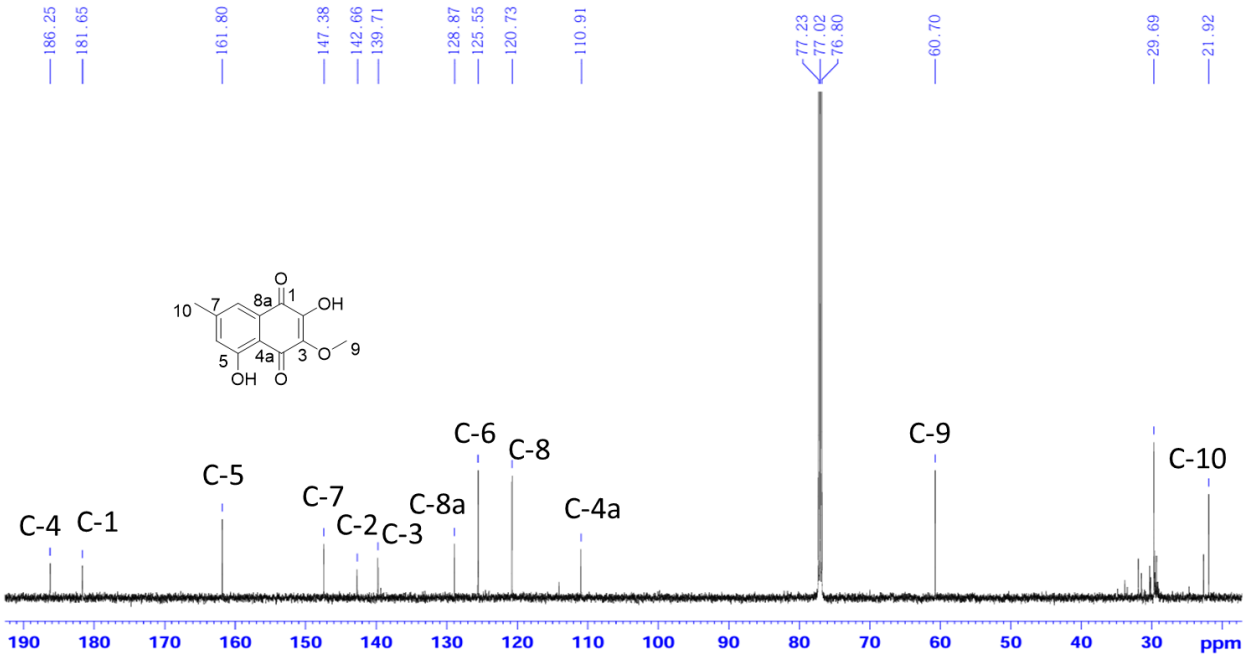


Figure S6 Expanded ^{13}C-NMR (150 MHz, $CDCl_3$) spectrum of compound 1 (Nepenthone C) (from δ_C 20 ppm to δ_C 190 ppm). The carbon chemical shifts were consistent with those reported for nepenthone C.

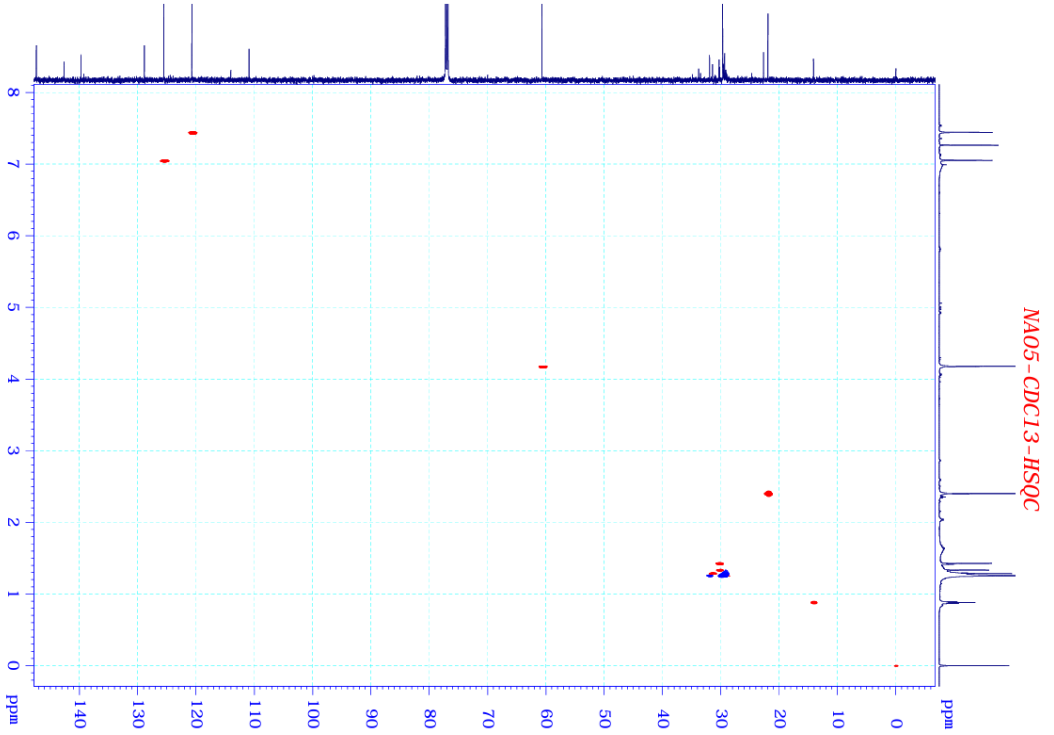


Figure S7 HSQC spectrum of compound 1 (Nepenthone C). The HSQC spectrum shows one-bond $^{1}H–^{13}C$ correlations of compound 1. These correlations helped assign the protonated carbons, including aromatic, methoxy, and methyl carbon signals.

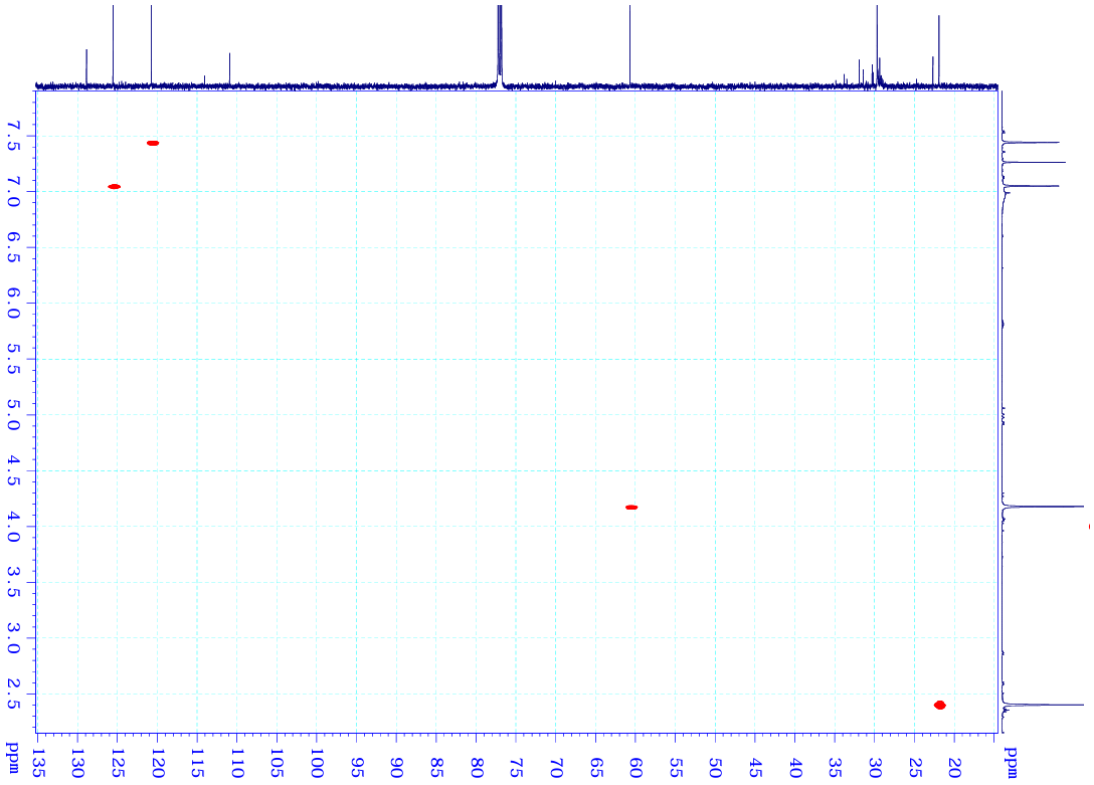


Figure S8 HSQC spectrum of compound 1 (Nepenthone C) (expanded no.1). The expanded HSQC spectrum provides a clearer view of the key $^{1}H–^{13}C$ correlations used for signal assignment. These data support the structural elucidation of compound 1 as nepenthone C.

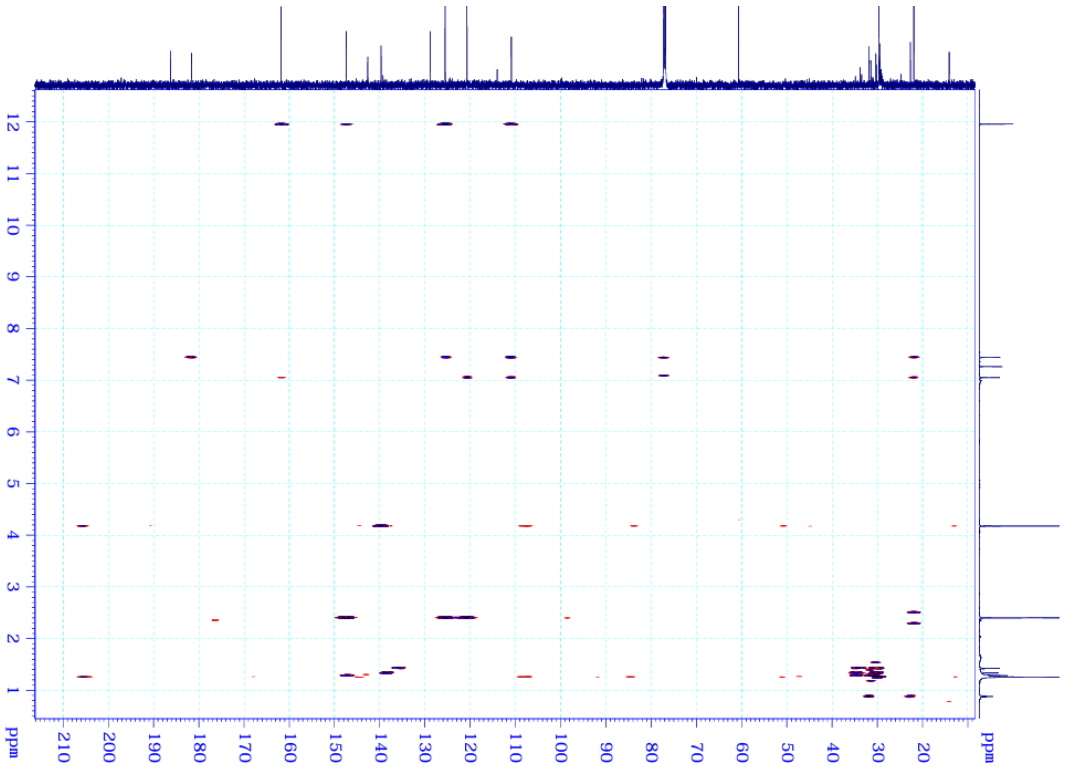


Figure S9 HMBC spectrum of compound 1 (Nepenthone C). These correlations were used to confirm the substitution pattern of the naphthoquinone nucleus.

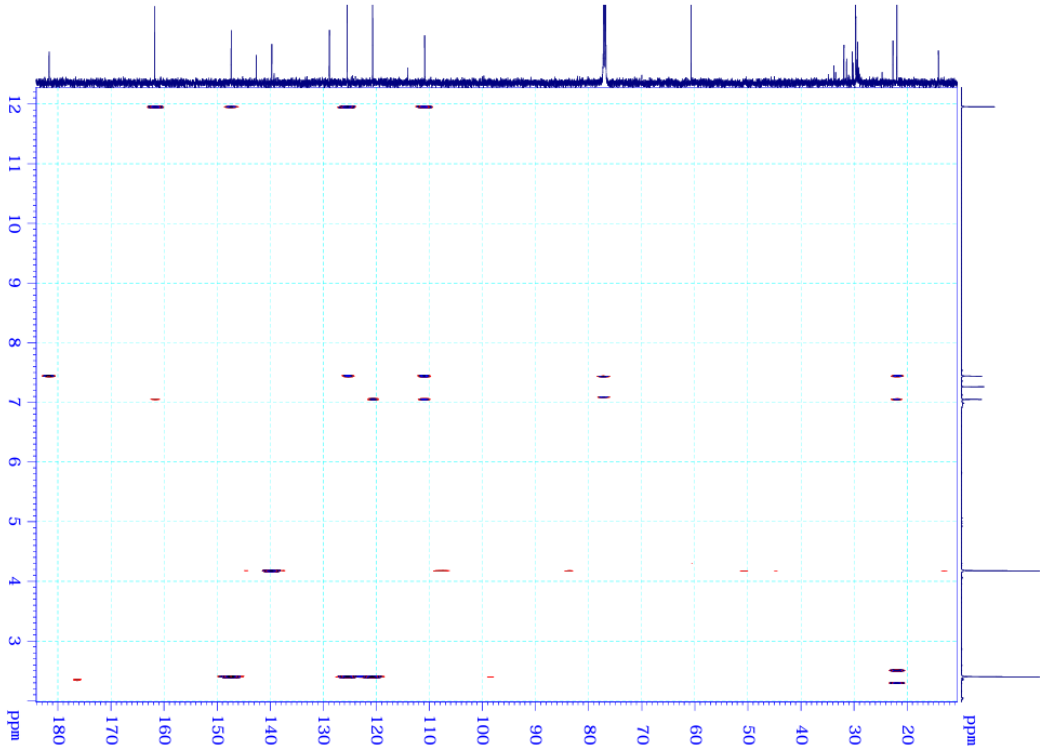


Figure S10 HMBC spectrum of compound 1 (Nepenthone C) (expanded no.1). This expanded HMBC region highlights selected long-range correlations relevant to the assignment of aromatic and quinone carbon signals. The observed correlations support the proposed naphthoquinone framework of compound 1.

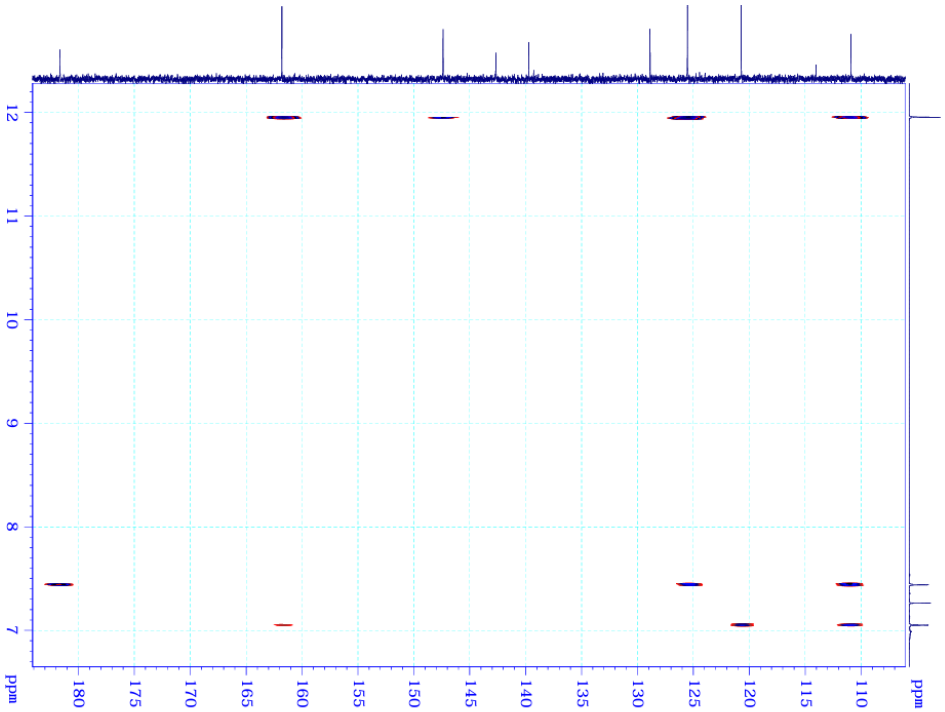


Figure S11 HMBC spectrum of compound 1 (Nepenthone C) (expanded no.2). This expanded HMBC region shows additional long-range correlations used to assign the methoxy and methyl substituents. These data further support the structural assignment of compound 1 as nepenthone C.

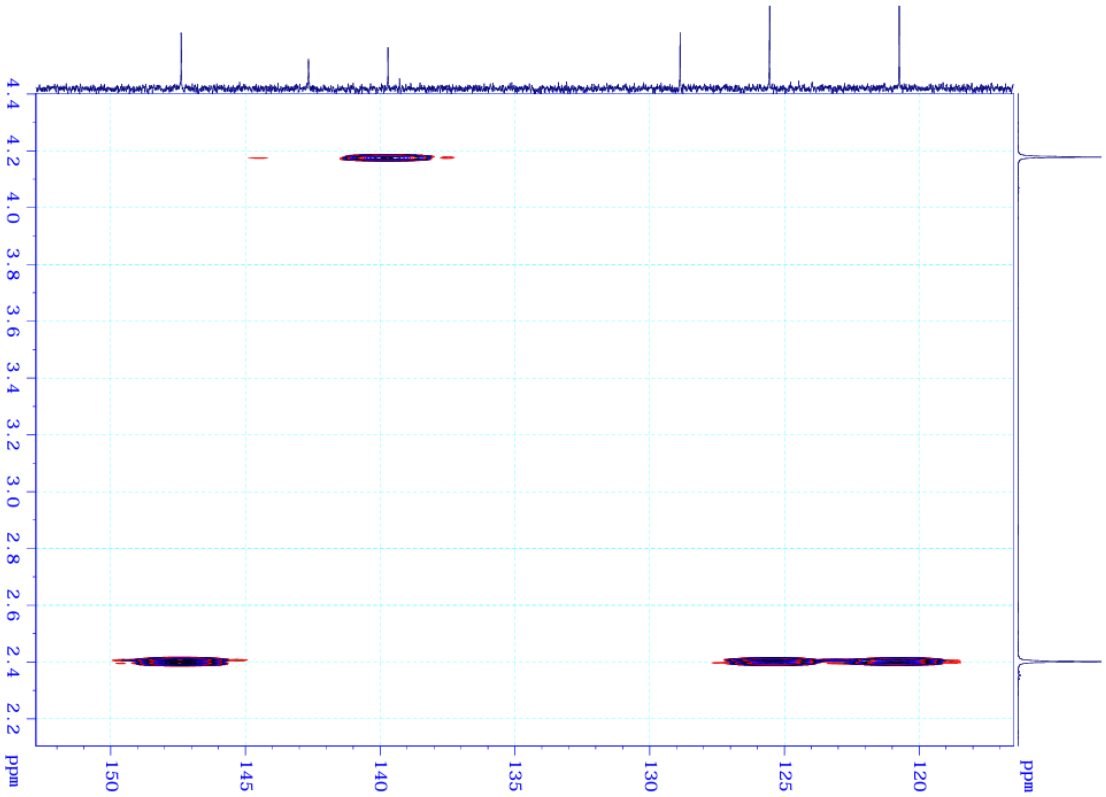


Figure S12 HMBC spectrum of compound 1 (Nepenthone C) (expanded no.3). This expanded HMBC region provides supporting long-range correlations for the substituted aromatic ring of compound 1. The correlations are consistent with the reported structure of nepenthone C.

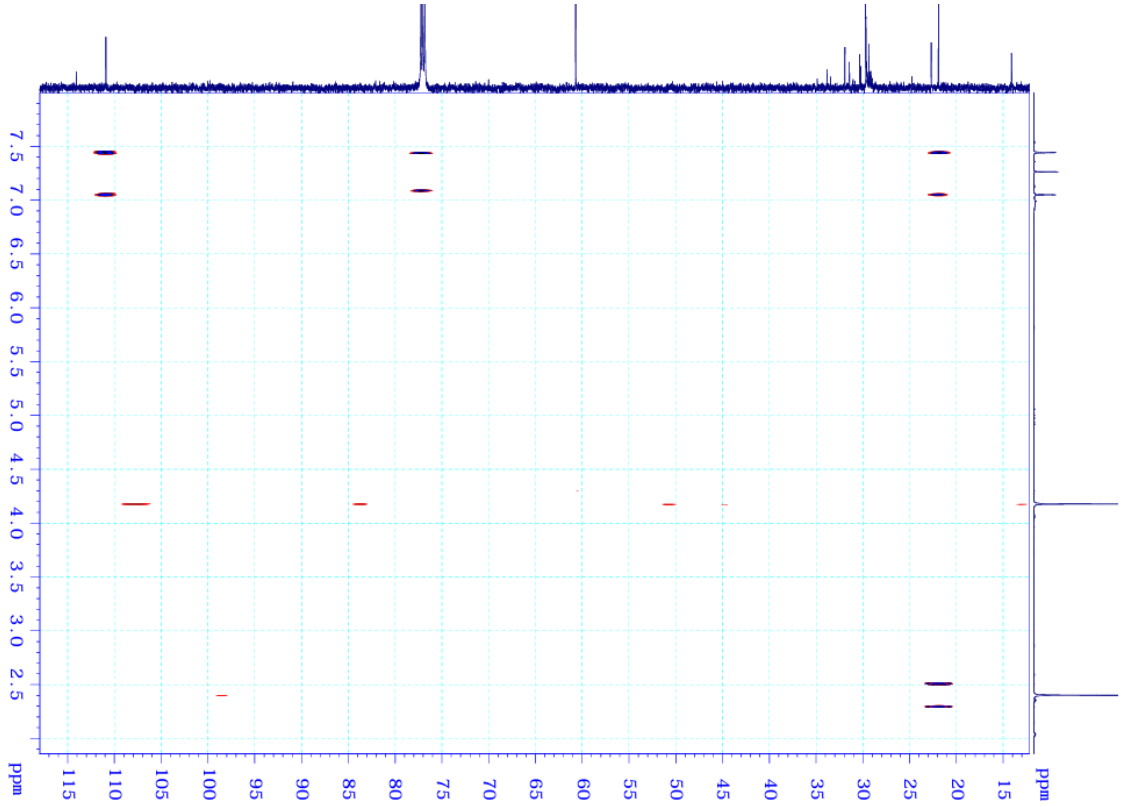


Figure S23 HMBC spectrum of compound 1 (Nepenthone C) (expanded no.4). This expanded HMBC region further illustrates key diagnostic correlations used in the structural elucidation of compound 1. Together with ^{1}H-NMR, ^{13}C-NMR, HSQC, and HRMS data, the HMBC results support the identification of compound 1 as nepenthone C.

Supplementary spectroscopic data of compound 2

Table S2 The comparison of NMR data of compound 2 with a similar compound (Quercetin).

Position	Compound 2 (DMSO-d_6)		Quercetin (CD_3OD) [3]	
	^{1}H-NMR (600 MHz) δ_H ppm	^{13}C-NMR (150 MHz) δ_C ppm	^{1}H-NMR (500 MHz) δ_H ppm	^{13}C-NMR (125 MHz) δ_C ppm
2	-	147.6	-	148.6
3	-	135.7	-	137.2
4	-	175.8	-	177.3
5	-	160.7	-	162.6
6	6.19 (1H, *d*, *J* = 1.8 Hz)	98.1	6.20 (1H, d, J = 2.0 Hz)	99.1
7	-	163.8	-	165.6
8	6.40 (1H, *d*, *J* = 1.8 Hz)	93.3	6.41 (1H, d, J = 2.0 Hz)	94.4
9	-	156.1	-	158.2
10	-	103.0	-	104.5
1'	-	121.9	-	124.1
2'	7.67 (1H, *d*, *J* = 1.8 Hz)	115.0	7.75 (1H, *d*, *J* = 2.0 Hz)	116.0
3'	-	145.0	-	146.2
4'	-	146.8	-	148.0
5'	6.89 (1H, *d*, *J* = 8.4 Hz)	115.5	6.90 (1H, d, J = 8.5 Hz)	116.2
6'	7.54 (1H, *dd*, *J* = 9.0, 2.4 Hz)	119.9	7.65 (1H, dd, J = 8.5; 2.0 Hz)	121.7

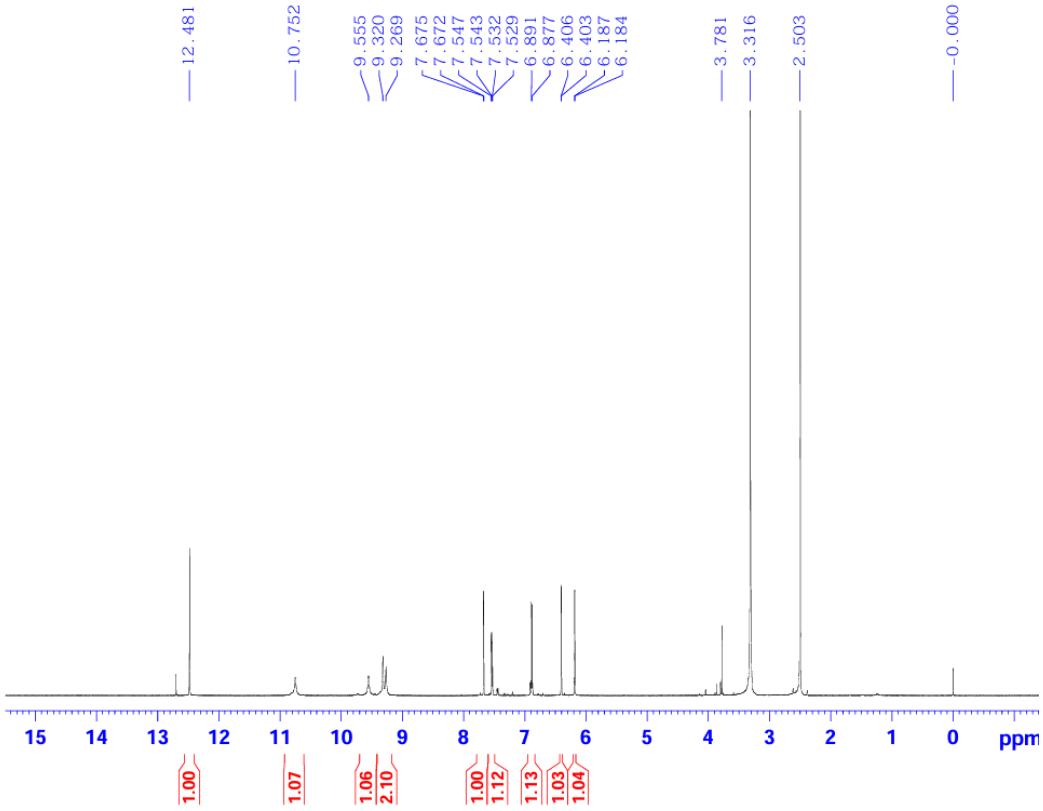


Figure S14 [1]H-NMR (600 MHz, DMSO-d_6) spectrum of compound 2 (Quercetin). The aromatic proton signals were consistent with the characteristic pattern of quercetin and supported the assignment of compound 2.

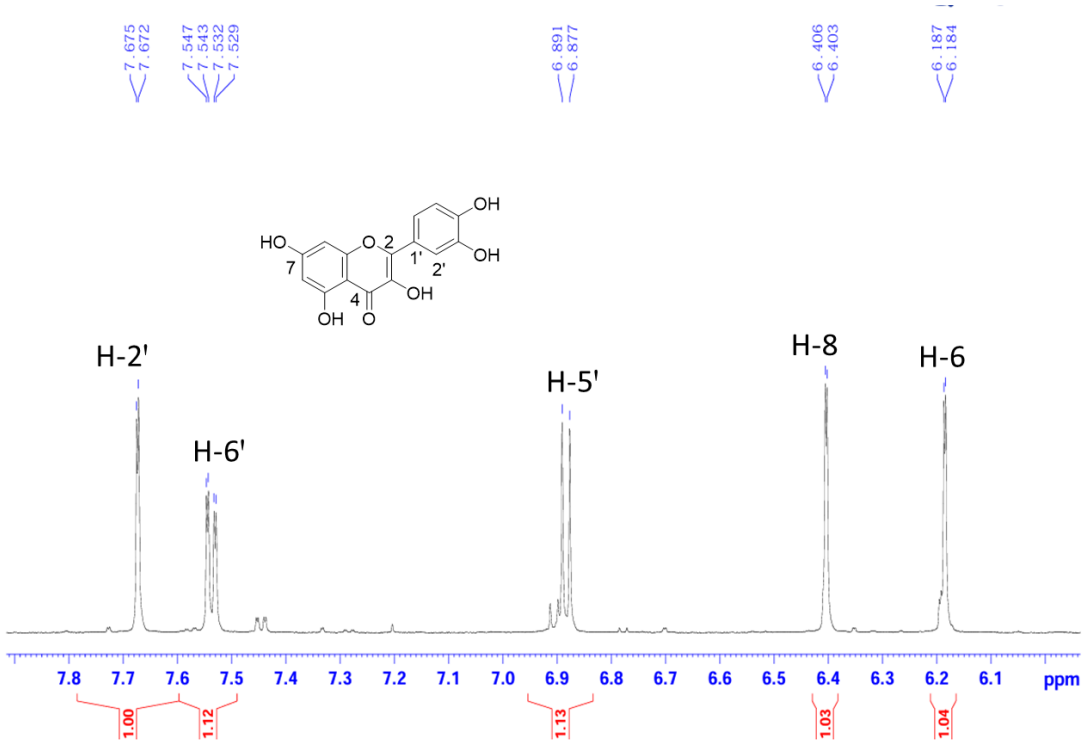


Figure S15 [1]H-NMR (600 MHz, DMSO-d_6) spectrum of compound 2 (Quercetin) (from δ_H 6 ppm to δ_H 13 ppm). The expanded [1]H-NMR spectrum from δ_H 6.0 to 13.0 ppm highlights the aromatic and phenolic proton regions of compound 2. These signals were used for comparison with reported quercetin data.

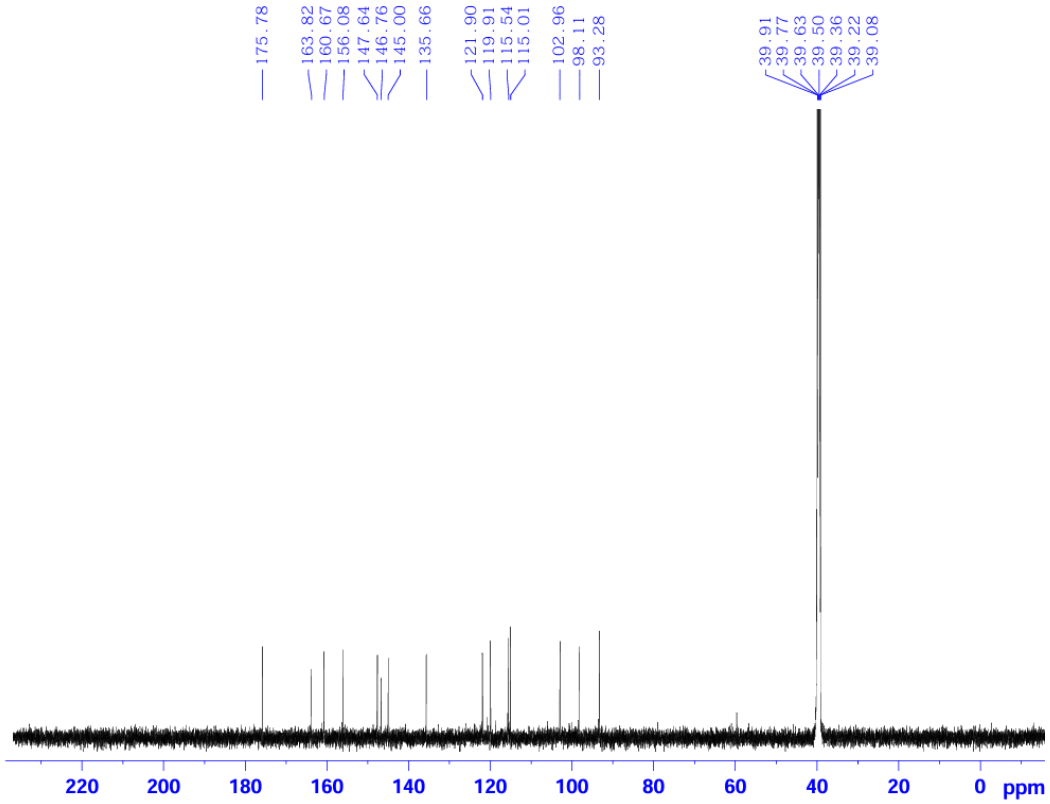


Figure S16 ^{13}C-NMR (150 MHz, DMSO-d_6) spectrum of compound 2 (Quercetin). The observed carbon resonances, including flavonoid carbonyl, oxygenated aromatic, and aromatic carbon signals, are consistent with the structure of quercetin.

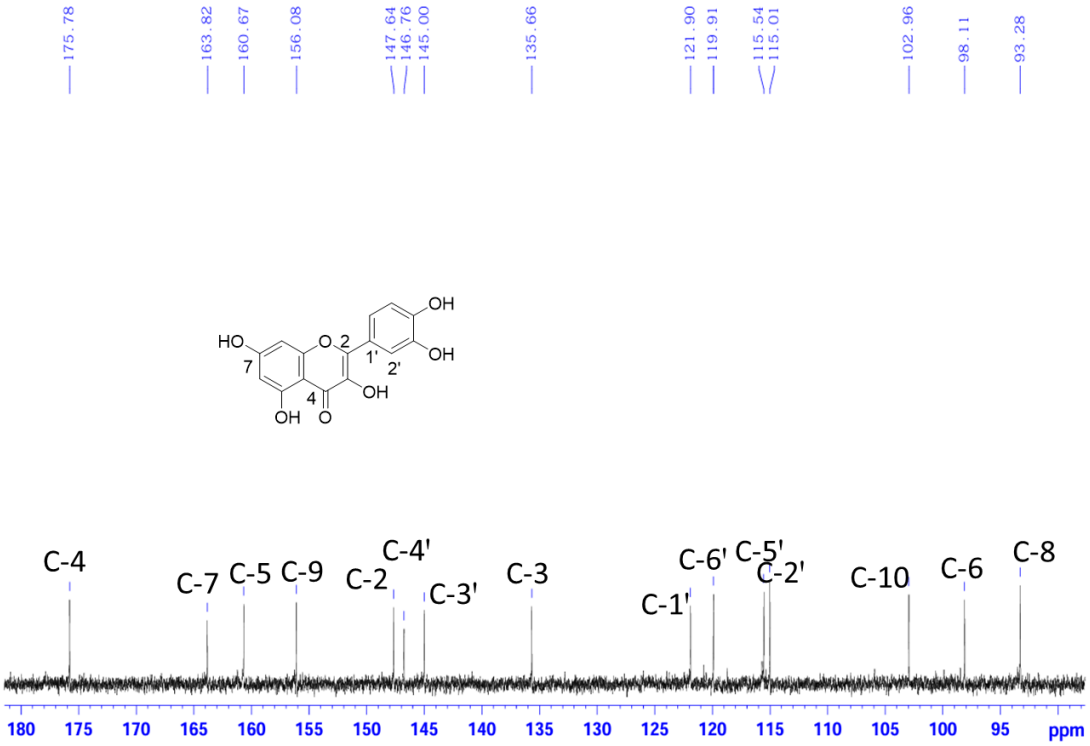


Figure S17 ^{13}C-NMR (150 MHz, DMSO-d_6) spectrum of compound 2 (Quercetin) (from δ_C 90 ppm to δ_C 180 ppm). The expanded ^{13}C-NMR spectrum from δ_C 90 to 180 ppm shows the key carbon resonances of the flavonoid skeleton. These data support the structural assignment of compound 2 as quercetin.

Supplementary spectroscopic data of compound 3

Table S3 The comparison of NMR data of compound 3 with a similar compound (Gallic acid).

Position	Compound 3 (CD_3OD)		Gallic acid (CD_3OD) [4]	
	^{1}H-NMR (600 MHz) δ_H ppm	^{13}C-NMR (150 MHz) δ_C ppm	^{1}H-NMR (500 MHz) δ_H ppm	^{13}C-NMR (125 MHz) δ_C ppm
1	-	122.0	-	122.1
2,6	7.08 (2H, s)	110.3	7.06 (2H, s)	110.5
3,5	-	146.4	-	146.5
4	-	139.6	-	139.3
7	-	170.4	-	170.6

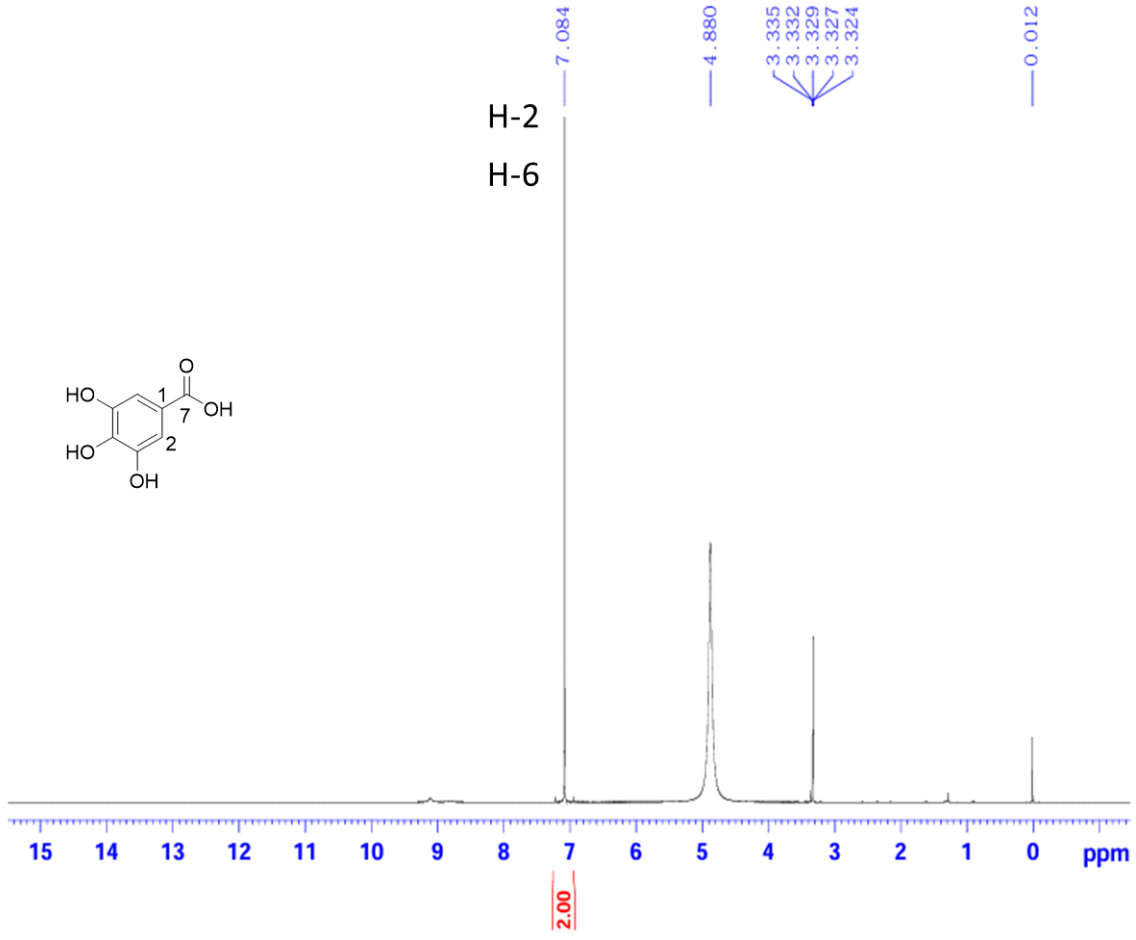


Figure S38 ^{1}H-NMR (600 MHz, CD_3OD) spectrum of compound 3 (Gallic acid). The singlet aromatic proton signal was consistent with the symmetrical aromatic structure of gallic acid.

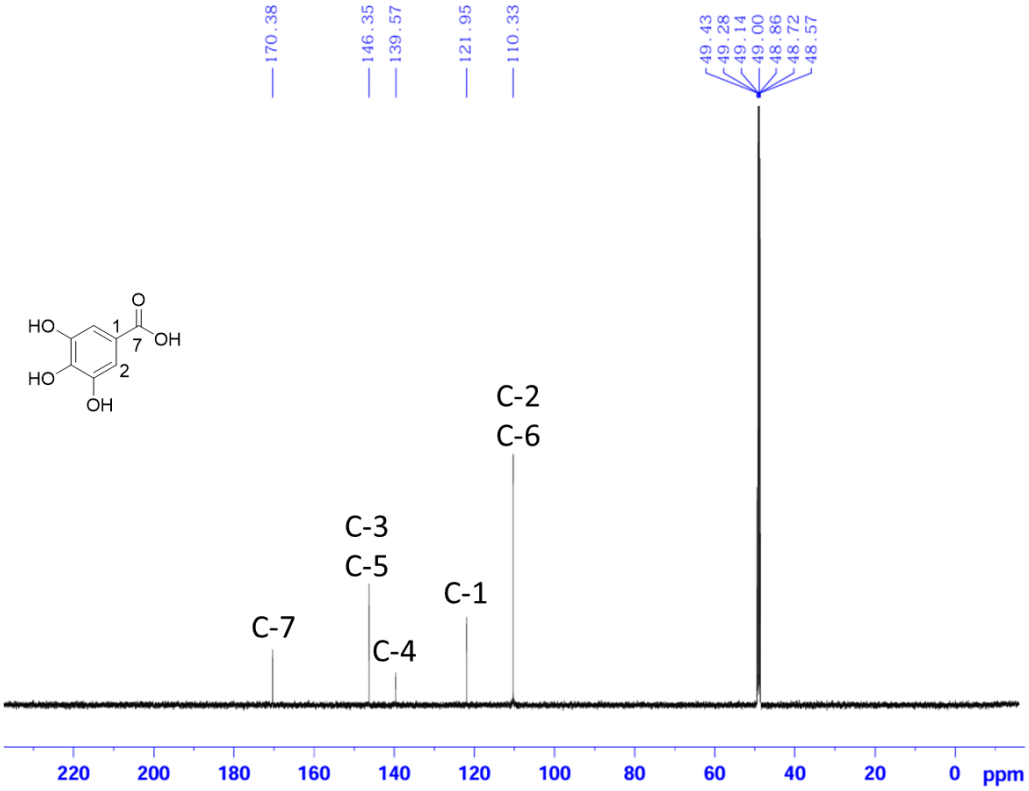


Figure S19 13C-NMR (150 MHz, CD3OD) spectrum of compound 3 (Gallic acid). The 13C-NMR spectrum was recorded at 150 MHz in CD3OD. The observed carbonyl and oxygenated aromatic carbon signals support the assignment of compound 3 as gallic acid.

Supplementary spectroscopic data of compound 4

Table S4 The comparison of the NMR data of compound 4 with a similar compound (Daucosterol).

Position	Compound 4 (DMSO-*d*$_6$)	Daucosterol (DMSO-*d*$_6$) [5]
	^{1}H-NMR (600 MHz) δ_H ppm	^{1}H-NMR (500 MHz) δ_H ppm
3	3.48 (1H, *m*)	3.50 (1H, *m*)
6	5.32 (1H, *s*)	5.35 (1H, *brs*)
18	0.65 (3H, *s*)	0.65 (3H, *s*)
19	0.96 (3H, *s*)	0.95 (3H, *s*)
21	0.90 (3H, *d*, J = 6.0 Hz)	0.90 (3H, *d*, J = 6.5 Hz)
26	0.83 (*m*)	0.82 (3H, *s*)
27	0.81 (*m*)	0.83 (3H, *s*)
29	0.80 (*m*)	0.79 (3H, *t*, J = 7.0)

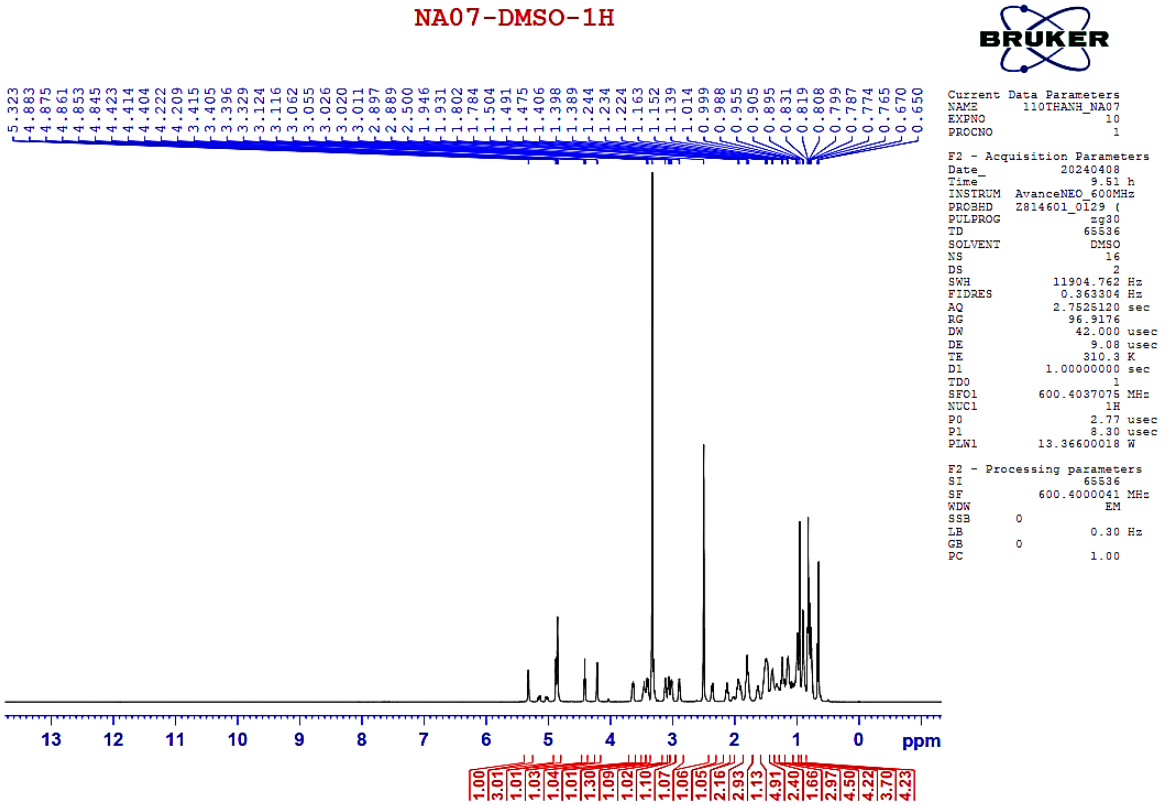


Figure S20 ^{1}H-NMR (600 MHz, DMSO-d_6) spectrum of compound 4 (Daucosterol). The characteristic steroidal proton signals, including olefinic, oxymethine, sugar, and methyl proton resonances, support the assignment of compound 4 as daucosterol.

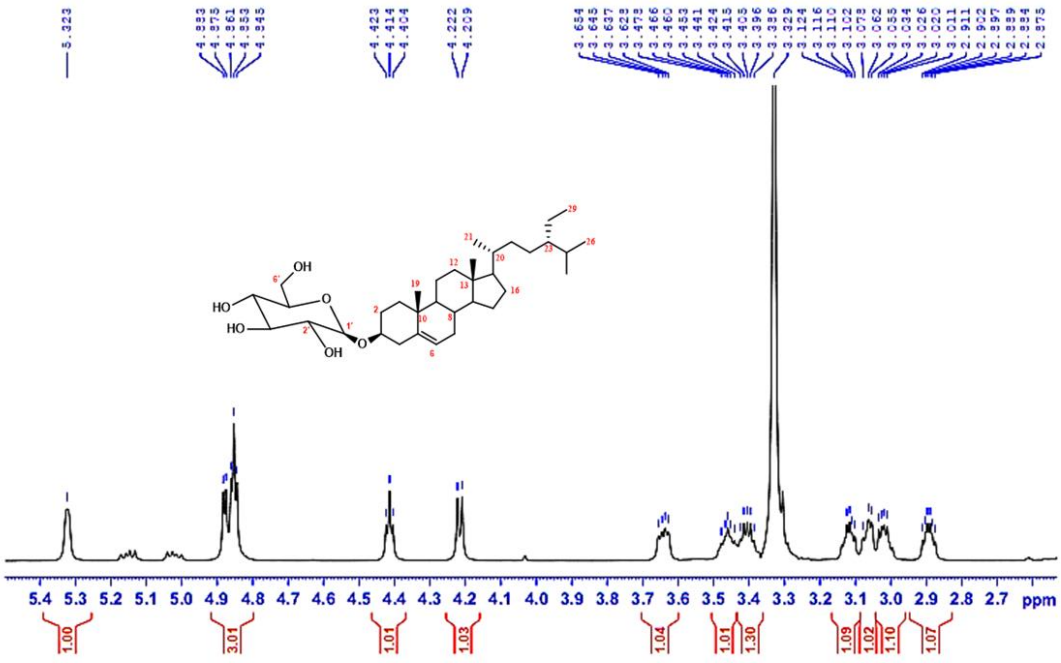


Figure S21 ^{1}H-NMR (600 MHz, DMSO-d_6) spectrum of compound 4 (Daucosterol) (from δ_H 2 ppm to δ_H 5.5 ppm). The expanded ^{1}H-NMR spectrum from δ_H 2.0 to 5.5 ppm highlights the oxymethine, olefinic, and glycosidic proton signals of compound 4. These diagnostic signals are consistent with the glucosylated sterol structure of daucosterol.

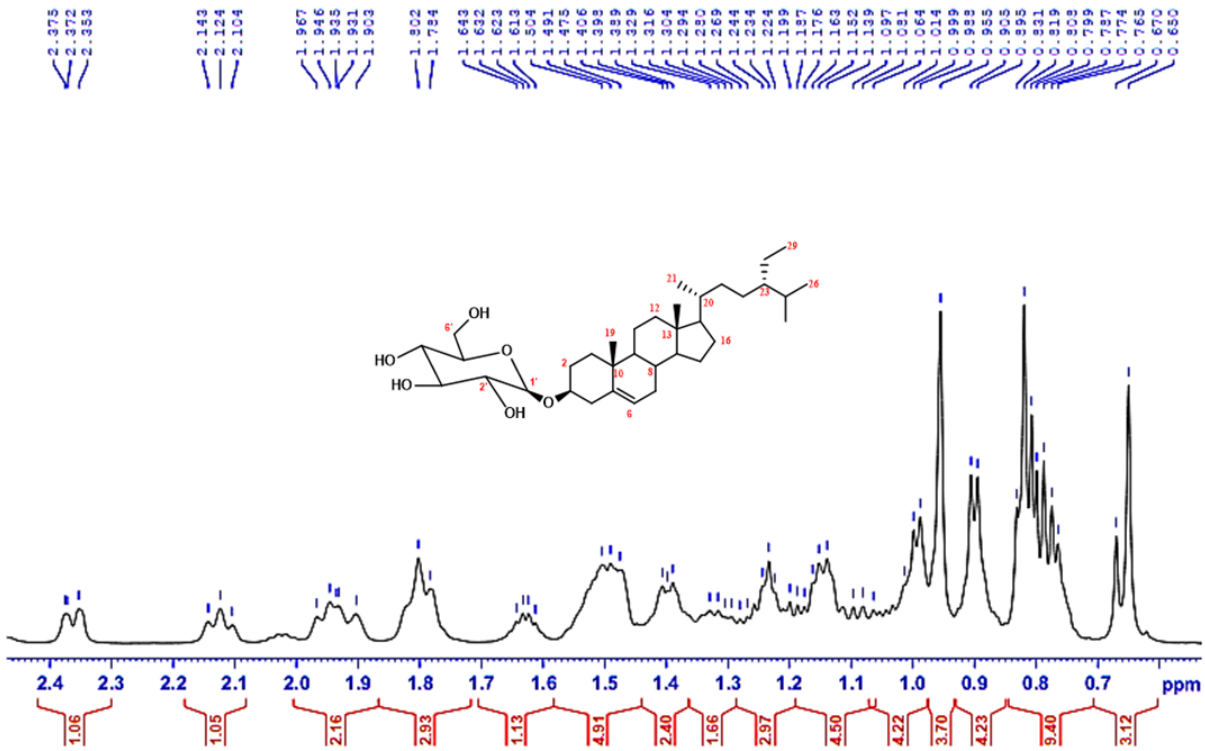


Figure S42 ^{1}H-NMR (600 MHz, DMSO-d_6) spectrum of compound 4 (Daucosterol) (from δ_H 0 ppm to δ_H 2 ppm). The expanded ^{1}H-NMR spectrum from δ_H 0 to 2.0 ppm shows the aliphatic and methyl proton signals of the steroidal skeleton. These signals further support the identification of compound 4 as daucosterol.

References

[1] TT Hong, VT Khang, NT Tuan and TQC Nguyen. Bioactivity-guided identification of constituents responsible for the anti-oxidative stress effects of *Nepenthes mirabilis*. *Records of Natural Products* 2026; **20(5)**, e26043785.

[2] SM Ryu, H Nam, JS Kim, J Song, YH Seo, HS Kim, AY Lee, WJ Kim, D Lee, BC Moon and J Lee. Chemical constituents of the egg cases of *Tenodera angustipennis* (Mantidis ootheca) with intracellular reactive oxygen species scavenging activity. *Biomolecules* 2021; **11(4)**, 556.

[3] NTH Van, PC Bach, CT Ich, DL Phuong, LT Thanh, TQ Toan and PQ Long. Flavonoids isolated from the flowers of *Camellia chrysantha*. *Vietnam Journal of Science and Technology* 2019; **57(3)**, 287-293.

[4] N Dang-Minh-Chanh, S Dong-Jun, L Hyang-Burm, K In-Seon, K Kil-Yong, P Ro-Dong and J Woo-Jin. Antifungal activity of gallic acid purified from *Terminalia nigrovenulosa* bark against *Fusarium solani*. *Microbial Pathogenesis* 2013; **56**, 8-15.

[5] VT Huyen, DTT Ai and NT Hien. Chemical constituents of leaves *Dialium cochinchinense* Pierre. *Vietnam Journal of Agricultural Sciences* 2021; **4(3)**, 1131-1136.